# *Unified numerical model for performance analysis of various cross-sections of concrete-filled stainless-steel tubular stub columns under axial loading*

Structures 55 (2023) 799–817

Contents lists available at ScienceDirect

Structures

journal homepage: www.elsevier.com/locate/structures

# Unified numerical model for performance analysis of various cross-sections of concrete-filled stainless-steel tubular stub columns under axial loading

Mizan Ahmed [a,*], Qing Quan Liang [b], Vipulkumar Ishvarbhai Patel [c], Soheil Gohari [d], Ahmed Hamoda [e]

[a] School of Civil and Mechanical Engineering, Curtin University, Kent Street, Bentley, WA 6102, Australia
[b] College of Sport, Health, and Engineering, Victoria University, PO Box 14428, Melbourne, VIC 8001, Australia
[c] School of Computing, Engineering and Mathematical Sciences, La Trobe University, Bendigo, VIC 3552, Australia
[d] Department of Mechanical Engineering, The University of Melbourne, Parkville, Victoria 3010, Australia
[e] Civil Engineering Dept., Faculty of Engineering, Kafrelsheikh University, Kafrelsheikh, Egypt

ARTICLE INFO

*Keywords:*
Unified model
Stainless Steel
Concrete-filled tubes
Performance analysis
Axial loading
Confined concrete
Computer program
Design formula

ABSTRACT

This research presents a unified numerical model for analyzing the performance of concrete-filled stainless-steel tubular (CFSST) stub columns with different cross-sectional shapes. The model converts the cross-sections of the CFSST columns with various shapes into an equivalent circular column, and a new concrete constitutive relation is proposed to estimate the compressive strength of confined concrete of CFSST columns with different cross-sections. To simulate the axial load–strain curves of CFSST columns, a computer program is used that converts the various cross-sections of CFSST columns into equivalent circular columns. To validate the model, 196 tested columns with various cross-sections gathered from previous literature are used. The unified model proposed is found to be accurately predicting the performance of CFSST columns. The model is then used to investigate the effects of concrete, steel yield stress, and the depth-to-thickness ratio on the different radius ratios and aspect ratios of CFSST columns. A unified design formula is also suggested to calculate the ultimate strength of CFSST columns with various shapes, and the proposed simplified model is shown to provide a more accurate estimation when compared to existing design codes.

## 1. Introduction

Concrete-filled steel tubular (CFST) columns are a popular choice for constructing high-rise buildings and bridge piers that need to carry large axial loads. They are preferred due to their strength, ductility, excellent fire, and cyclic performance than that of reinforced concrete columns. The steel tube provides lateral confinement to the confined concrete and serves as formwork during construction. Many studies have been conducted on CFST columns, leading to a better understanding of their design, and the availability of design guidelines in various publications [1–10]. Circular columns offer more uniform confinement compared to rectangular ones [11], but rectangular columns are easier to connect to adjacent beams. To achieve both a higher strength and ease of connection to adjacent beams, other cross-sections such as round-ended, octagonal, elliptical and hexagonal columns have also been proposed [12–25].

CFST columns encounter corrosion in an acidic environment, which can significantly affect their performance. To address this issue, concrete-filled stainless-steel tubular (CFSST) columns have been proposed. These columns offer improved corrosion resistance, hardness, strength, and ductility due to the strain hardening performance of strain-hardening which is superior to that of carbon steel used in conventional CFST columns. However, due to the higher cost of stainless steel, the use of CFSST columns is limited. Researchers have conducted experimental work to examine the structural performance of CFSST columns, but design guidelines for CFSST columns are not yet available in Eurocode 4 [26], AISC 360–16 [27], ACI 318–19 [28] and DBJ 13–51-2010 [29]. Therefore, understanding the effects of stainless steel on the cost-effective design of these columns is crucial.

Numerous studies on CFSST columns have been documented in the literature, investigating their behavior under various loading conditions [30–51]. Young and Ellobody [30] studied the effects of sectional shapes, concrete strength, and loading type on the performance of CFSST columns. Lam and Gardner [31] found that CFSST columns made

* Corresponding author.
*E-mail address:* mizan.ahmed@curtin.edu.au (M. Ahmed).

https://doi.org/10.1016/j.istruc.2023.06.079
Received 11 May 2023; Received in revised form 13 June 2023; Accepted 15 June 2023
Available online 22 June 2023

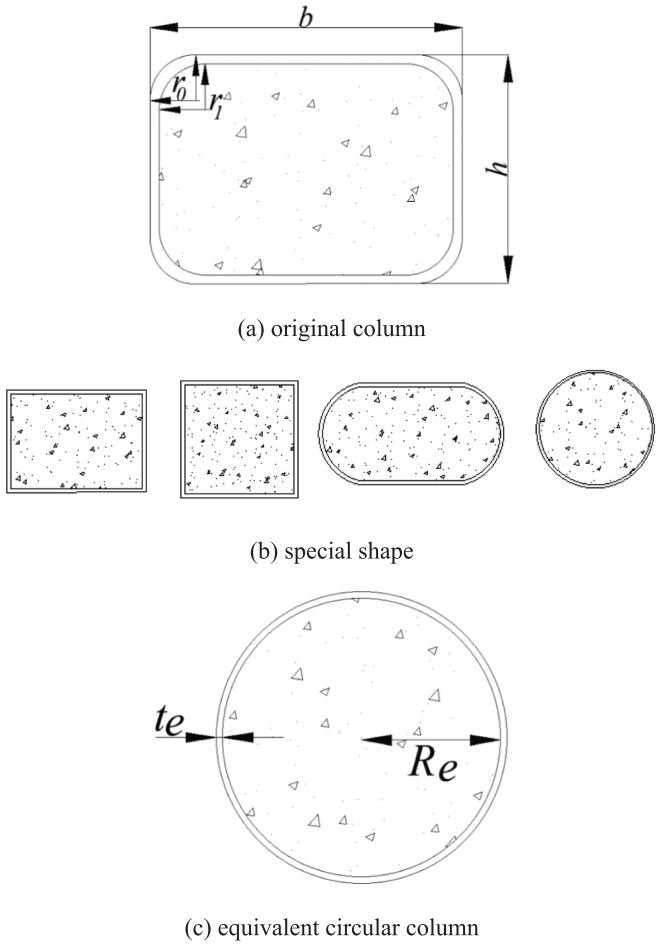


**Fig. 1.** Transformation of various shapes to an equivalent circular column.

with high-strength concrete (HSC) had poor ductility due to the brittle nature of HSC. Uy et al. [32] conducted extensive tests on CFSST columns with circular and rectangular shapes and analyzed the influence of loading types, cross-sectional shapes, concrete strength, column slenderness, and steel tube thickness on their performance. The circular CFSST columns exhibited higher strength and ductility than the rectangular ones. Tam et al. [40] reported that using a higher percentage of recycled aggregates in CFSST columns decreased their load-carrying capacity. Liao et al. [45] investigated the impact of different types of sand used in the concrete of CFSST columns. They found that the type of sand has insignificant influences on CFSST columns. Azad et al. [52,53] proposed formulas for determining the slenderness limit and effective diameter of CFSST columns based on their test results. Liu et al. [54] studied the size effects of CFSST stub columns under axial loading. It was concluded that the size effects of CFSST stub columns decrease as the steel ratio increases. Zhong and Zhao [55] performed tests on eccentrically loaded CFSST stub columns containing recycled aggregates. It was found that the effects of various percentages of recycled aggregates were negligible on the performance of CFSST stub columns under eccentric loading. Han et al. [56] also performed tests on CFSST columns containing recycled aggregates. It was found that the bond strength of CFSST columns containing recycled aggregates was lower than that of normal CFSST columns.

Researchers have previously developed computational models to investigate the behavior of CFSST columns, as reported in various studies [25,48,57–67]. The accuracy of these numerical models depends on how well they simulate the material behavior of CFSST columns. However, according to Ahmed et al. [66], existing numerical models of CFSST columns use confinement models designed for conventional CFST columns, which may lead to inaccurate performance predictions. Tran et al. [68] examined the accuracy of various machine learning models in predicting the ultimate strength of circular CFSST columns under axial loading. In addition, 3D finite element models (FEM) are time-consuming and cannot account for local buckling, unlike the fiber models developed by Liang [69], Patel et al. [70] and Ahmed et al. [64,71]. Some researchers have proposed unified models for CFST columns, including Lin et al. [72,73] and Min et al. [74–76], while Lam and Teng [77] and Légeron and Paultre [78] have used a unified method to convert rectangular columns to equivalent circular columns to predict the performance of concrete columns. Although the unified model proposed by Lin et al. [72] provides good prediction of the performance of CFST columns with carbon tube but does not accurately predict the performance of CFSST columns, as it ignores the strain-hardening performance of stainless steel. Moreover, the concrete compressive strength formula proposed by Attard and Setunge [79], which was modified by incorporating a shape factor in the unified modeling, does not accurately predict the performance of CFSST columns due to the different confinement mechanisms of steel-confined concrete columns.

This paper introduces a novel unified numerical model to predict the performance of CFSST columns of different shapes, including rectangular, square, circular, and round-ended. The model converts the cross-sections of various shapes of CFSST columns into an equivalent circular column. The model is based on a database of 196 columns, which includes different cross-sections of CFSST and CFST columns. It should be noted that the length-to-width ($L/b$) ratio of the columns collected in the database are limited to 4 to avoid the effects of global buckling on their axial performance. The new concrete constitutive relation for estimating the compressive strength of confined concrete is developed, along with a strength reduction factor to capture the post-peak performance of confined concrete. A computer program is then created, which includes the newly proposed concrete confinement model and accurate three-stage constitutive relations of stainless steel to develop axial load–strain curves of CFSST columns. The program also converts various cross-sections of CFSST columns into equivalent circular columns. The accuracy of the proposed unified model is verified against a large test data. Finally, a unified design formula is proposed to calculate the ultimate strength of CFSST columns of different shapes.

## 2. The unified numerical model

### 2.1. Equivalent circular column

The unified model proposed in this paper takes into consideration various cross-sectional shapes of CFSST columns, such as circular, rectangular, square, and round-ended. The study assumes that these shapes are special cases of rectangular columns, as depicted in Fig. 1 [72,77]. In the model, the cross-sections of these different shapes are converted into an equivalent circular column, as shown in Fig. 1. The width and depth of the column are represented by $b$ and $h$, respectively, where $b$ is greater than or equal to $h$. The thickness of the steel tube is represented by $t$, and the outer and inner radius of the steel tube are represented by $r_0$ and $r_1$, respectively. If $r_0 = r_1 = 0$ and $b \geq h$, then it is a rectangular column, while $r_0 = r_1 = 0$ and $b = h$ represents a square column. For $r_0 = h/2, r_1 = h/2 - t$ and $b = h$ refers to the circular column and $r_0 = h/2, r_1 = h/2 - t$ and $b > h$ refers to the column as round-ended. The performance analysis of axially loaded CFSST columns is carried out using the equivalent circular column. It should be noted that Lam and Teng [77], and Légeron and Paultre [78] developed unified models for conventional reinforced concrete columns where the cross-sectional area of the equivalent circular column was different from that of the original shape of the column. However, in this study, a unified model is developed for CFSST columns where the cross-sectional area of the steel tube and confined concrete of the original column is the same as that of the equivalent circular column. The cross-sectional area of the steel tube and confined concrete of the equivalent circular column are calculated

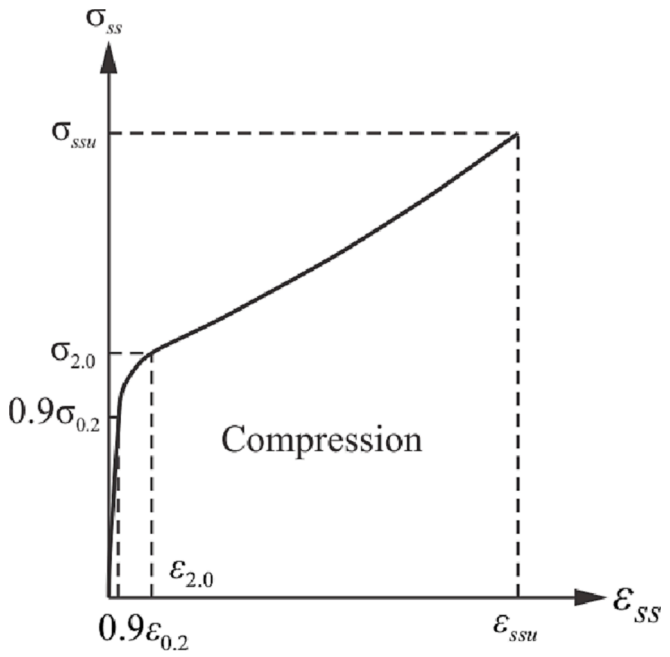


**Fig. 2.** Constitutive relations of stainless steel under compression.

using Eqs. (1–2).

$$A_c = \pi R_e^2 = (b-2t)(h-2t) - (4-\pi)r_1^2 \tag{1}$$

$$A_s = \pi\left[(R_e + t_e)^2 - R_e^2\right] = 2t(b+h) - 4t^2 - (4-\pi)(r_0^2 - r_1^2) \tag{2}$$

where the wall thickness of the tube and the radius of the confined concrete of the equivalent circular column are characterized by $t_e$ and $R_e$, respectively.

By solving Eqs. (1) and (2), $R_e$ and $t_e$ can be calculated as

$$R_e = \sqrt{\frac{(b-2t)(h-2t) - (4-\pi)r_1^2}{\pi}} \tag{3}$$

$$t_e = \frac{\sqrt{bh - (4-\pi)r_0^2} - \sqrt{(b-2t)(h-2t) - (4-\pi)r_1^2}}{\sqrt{\pi}} \tag{4}$$

### 2.2. Analysis steps

A unified numerical model is developed here to predict the axial load–strain curves of axially loaded CFSST columns. The model takes into account the areas of steel and concrete, as well as their corresponding stresses to determine the axial load. The model assumes that the plane section remains plane during plastic deformation, and that the steel and concrete are perfectly bonded. In addition, the effects of shrinkage and temperature are not considered. The stresses of steel and concrete are estimated from the axial strains employing the uniaxial constitutive relationships of steel and concrete given in the following sections. The axial force ($P$) of the column is taken as the stress resultant. In the analysis, the axial strain is increased incrementally and determined the axial load of the columns. The iteration procedure continues until the axial load is 50% of the maximum load or the maximum prescribed strain is attained.

The computational analysis for calculating the axial load–strain responses of CFSST short columns is as follows.

(1) Input the following parameters of CFSST columns: $b$, $h$, $t$, $r_0$, $r_1$, $\sigma_{0.2}$ and $f_c'$.
(2) Determine $R_e$ and $t_e$ using Eqs. (3) and (4), respectively.
(3) Calculate the area of steel and concrete using Eqs. (1) and (2), respectively.
(4) Initialize fiber axial strain as $\varepsilon = \Delta\varepsilon$.
(5) Determine the steel and concrete's stresses from the uniaxial constitutive material relationships.
(6) Compute the axial load ($P$) as $P = \sigma_s A_s + \sigma_c A_c$, where $\sigma_s$ and $\sigma_c$ are the stresses of steel and concrete, respectively; $A_s$ and $A_c$ are the area of steel and concrete, respectively.
(7) Increase the strain by $\varepsilon = \varepsilon + \Delta\varepsilon$.
(8) Repeat Steps (5) to (7) until $P \leq 0.5P_{\max}$ or $\varepsilon \geqslant \varepsilon_{cu}$.
(9) Plot $P - \varepsilon$ curve.

## 3. Material constitutive relations

### 3.1. Constitutive relations of stainless steel

The constitutive relationships of stainless steel in this study are determined using Quach et al.'s constitutive model [80], as depicted in Fig. 2. According to the literature, the three-stage stress–strain relationships of stainless steel in Fig. 2 yield more precise outcomes than the two-stage relationships such as Rasmussen's model [81]. In this study, the stress in stainless steel is computed from the corresponding strain using the formulas developed by Abdella et al. [82]. To account for the effects of welding, cold forming, and biaxial stress on the stainless-steel tube, a 10% reduction is applied to the 0.2% proof strength, which is considered as the yield strength of the stainless-steel tube [11,83]. It should be noted that the residual stress exists in the corner of the cold-formed steel tube with rectangular cross-sections due to the cold-forming has moderate effects on the ultimate strength of conventional CFST columns. However, all the CFSST columns collected for the validation of the unified model was constructed by welding the stainless-steel plates, therefore, the corner effects are neglected for this study. In addition, for the CFSST columns with rectangular flat plates, the local buckling formulas proposed by Liang et al. [84] considered the residual stress induced by welding.

In the first stage ($0 \leqslant \varepsilon_s \leqslant \varepsilon_{0.2}$) of the constitutive model, the stress is calculated as

$$\sigma_s = \frac{E_0\,\varepsilon_s\left[1 + C_1\left(\frac{\varepsilon_s}{\varepsilon_{0.2}}\right)^{C_2}\right]}{1 + C_3\left(\frac{\varepsilon_s}{\varepsilon_{0.2}}\right)^{C_4} + C_1\left(\frac{\varepsilon_s}{\varepsilon_{0.2}}\right)^{C_2}} \tag{5}$$

In which $\sigma_s$ and $\varepsilon_s$ are the stress of the steel fiber and the corresponding strain, respectively;$E_0$ is the Young's modulus of steel; $\sigma_{0.2}$ and $\varepsilon_{0.2}$ are the 0.2% proof stress of the stainless steel and the corresponding strain, respectively. Ramberg and Osgood [85] proposed formular for $\varepsilon_{0.2}$ written as

$$\varepsilon_{0.2} = \frac{\sigma_{0.2}}{E_0} + 0.002 \tag{6}$$

In Eq. (5), $C_1$, $C_2$, $C_3$ and $C_4$ are calculated as

$$C_1 = \frac{\Delta}{C_2 - 1} \tag{7}$$

$$C_2 = 1 + \frac{B_1}{\Delta} \tag{8}$$

$$C_3 = G_0(1 + C_1) \tag{9}$$

$$C_4 = \Delta + G_1 \tag{10}$$

where

$$\Delta = \frac{1 + \sqrt{1 + 4B_1}}{2} \tag{11}$$

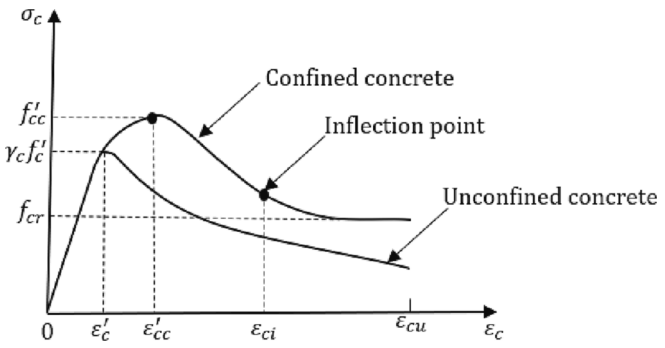


**Fig. 3.** Constitutive relations of confined and unconfined concrete.

$$B_1 = \frac{G_1 E_{0.2}(n+G_0)}{E_0} \tag{12}$$

$$G_0 = \frac{0.002E_0}{\sigma_{0.2}} \tag{13}$$

$$G_1 = \frac{\varepsilon_{0.2}E_{0.2}(n-1)}{\sigma_{0.2}} \tag{14}$$

$$E_{0.2} = \frac{E_0}{1+0.002\left(\frac{nE_0}{\sigma_{0.2}}\right)} \tag{15}$$

$$n = \frac{\ln\,(20)}{\ln\,(\sigma_{0.2}/\sigma_{0.01})} \tag{16}$$

where $n$ is the Knee factor and $E_{0.2}$ is the tangent modulus of the stainless steel at 0.2% proof strain.

The stress of stainless steel in the second stage $(\varepsilon_{0.2} < \varepsilon_s \leqslant \varepsilon_{2.0})$ is calculated as

$$\sigma_s = \sigma_{0.2} + \frac{E_{0.2}\left[1+C_5\left(\frac{\varepsilon_s-\varepsilon_{0.2}}{\varepsilon_{1.0}-\varepsilon_{0.2}}\right)^{C_6}\right](\varepsilon_s-\varepsilon_{0.2})}{1+C_7\left(\frac{\varepsilon_s-\varepsilon_{0.2}}{\varepsilon_{1.0}-\varepsilon_{0.2}}\right)^{C_8}+C_5\left(\frac{\varepsilon_s-\varepsilon_{0.2}}{\varepsilon_{1.0}-\varepsilon_{0.2}}\right)^{C_6}} \tag{17}$$

where $\sigma_{1.0}$ and $\varepsilon_{1.0}$ are the 1.0% proof stress and the corresponding strain, respectively. $\sigma_{1.0}$ and $\varepsilon_{1.0}$ were proposed by Quach et al. [80] as

$$\sigma_{1.0} = \sigma_{0.2}\left(\frac{0.662}{n}+1.085\right) \tag{18}$$

$$\varepsilon_{1.0} = \varepsilon_{0.2} + \frac{\sigma_{1.0}-\sigma_{0.2}}{E_{0.2}} + \left[0.008+(\sigma_{1.0}-\sigma_{0.2})\left(\frac{1}{E_0}-\frac{1}{E_{0.2}}\right)\right] \tag{19}$$

In Eq. (17), $C_5$, $C_6$, $C_7$ and $C_8$ are calculated as

$$C_5 = \frac{1}{C_6-1} \tag{20}$$

$$C_6 = C_8 + \frac{1}{\ln\left(\frac{\varepsilon_{2.0}-\varepsilon_{0.2}}{\varepsilon_{1.0}-\varepsilon_{0.2}}\right)}\left[\ln(1+A_2)+\ln\left(\frac{H_0}{H_2}\right)\right] \tag{21}$$

$$C_7 = H_0\,(1+C_5) \tag{22}$$

$$C_8 = 1+H_1 \tag{23}$$

where

$$A_2 = \frac{(n_2-1)^2\,(H_2-H_0)}{(1+n_2H_0)\,(1+n_2H_2)} \tag{24}$$

$$H_0 = \frac{\left[0.008+(\sigma_{1.0}-\sigma_{0.2})\left(\frac{1}{E_0}-\frac{1}{E_{0.2}}\right)\right]E_{0.2}}{\sigma_{1.0}-\sigma_{0.2}} > 0 \tag{25}$$

$$H_1 = \frac{(n_2-1)\,(H_0+1)}{1+n_2H_0} \tag{26}$$

$$H_2 = \frac{E_{0.2}(\varepsilon_{2.0}-\varepsilon_{0.2})}{\sigma_{2.0}-\sigma_{0.2}} - 1 \tag{27}$$

$$n_2 = 6.399\left(\frac{E_{0.2}}{E_0}\right)\left(\frac{\sigma_{1.0}}{\sigma_{0.2}}\right)+1.145 \tag{28}$$

where $\sigma_{2.0}$ and $\varepsilon_{2.0}$ are 2.0% proof stress and the corresponding strain, respectively. $\sigma_{2.0}$ and $\varepsilon_{2.0}$ are calculated using the formulas proposed by Quach et al. [80]:

$$\sigma_{2.0} = \sigma_{0.2}\left[\frac{1+\left(\frac{\sigma_{1.0}}{\sigma_{0.2}}-1\right)A^{\frac{1}{n_2}}}{1+\left(\frac{\sigma_{0.2}}{E_0}\right)\left(\frac{E_0}{E_{0.2}}-1\right)\left(\frac{\sigma_{1.0}}{\sigma_{0.2}}-1\right)\left(\frac{A^{\frac{1}{n_2}}}{n_2B_2}\right)}\right] \tag{29}$$

$$\varepsilon_{2.0} = \varepsilon_{0.2} + \frac{\sigma_{2.0}-\sigma_{0.2}}{E_{0.2}} + \left[0.008+(\sigma_{1.0}-\sigma_{0.2})\left(\frac{1}{E_0}-\frac{1}{E_{0.2}}\right)\right]\left(\frac{\sigma_{2.0}-\sigma_{0.2}}{\sigma_{1.0}-\sigma_{0.2}}\right)^{n_2} \tag{30}$$

where,

$$A = \frac{B_2}{0.008+\left(\frac{\sigma_{0.2}}{E_0}\right)\left(\frac{\sigma_{1.0}}{\sigma_{0.2}}-1\right)\left(1-\frac{E_0}{E_{0.2}}\right)} \tag{31}$$

$$B_2 = 0.018+\left(\frac{\sigma_{0.2}}{E_0}\right)\left(\frac{E_0}{E_{0.2}-1}\right) \tag{32}$$

The stress of stainless steel in the third stage $(\varepsilon_{2.0} < \varepsilon_s \leqslant \varepsilon_{su})$ is calculated as

$$\sigma_s = \frac{A_3+B_3\varepsilon_s}{1-\varepsilon_s} \tag{33}$$

where

$$A_3 = \sigma_{2.0}(1-\varepsilon_{2.0}) - B_3\varepsilon_{2.0} \tag{34}$$

$$B_3 = \frac{\sigma_{su}(1-\varepsilon_{su})-\sigma_{2.0}(1-\varepsilon_{2.0})}{\varepsilon_{su}-\varepsilon_{2.0}} \tag{35}$$

where $\sigma_{su}$ and $\varepsilon_{su}$ are the ultimate stress and the ultimate strain, respectively and can be calculated as:

$$\varepsilon_{uc} = 1-\frac{1}{1+\varepsilon_{ut}} \tag{36}$$

$$\sigma_{uc} = (1+\varepsilon_{ut})^2\sigma_{ut} \tag{37}$$

where $\sigma_{ut}$ and $\varepsilon_{ut}$ are the ultimate tensile strength and the ultimate tensile strain, respectively and calculated as

$$\sigma_{ut} = \sigma_{0.2}\left[\frac{1-0.0375(n-5)}{185e+0.2}\right] \tag{38}$$

$$\varepsilon_{ut} = 1-\frac{\sigma_{0.2}}{\sigma_{ut}} \tag{39}$$

### 3.2. Constitutive relations of concrete

Fig. 3 presents the constitutive relations of concrete adopted. The constitutive relations of concrete under compression are expressed as [86,87]:

**Table 1**
Validation of the accuracy of the unified model for circular CFSST columns.

| Specimen | $b(b=h)$ (mm) | $t$ (mm) | $L$ (mm) | $L/b$ | $\sigma_{0.2}$ (MPa) | $f_c^{'}$ (MPa) | $P_{u,\exp}$ (kN) | $P_{u,num}$ (kN) | $\frac{P_{u,num}}{P_{u,\exp}}$ | $P_{u,Lin}$ (kN) | $\frac{P_{u,Lin}}{P_{u,\exp}}$ | Ref. |
|---|---|---|---|---|---|---|---|---|---|---|---|---|
| CHS104 × 2-C30 | 104.0 | 2.0 | 312 | 3.0 | 412 | 31 | 699 | 663 | 0.95 | 648 | 0.93 | [31] |
| CHS114 × 6-C60 | 114.3 | 6.0 | 343 | 3.0 | 266 | 49 | 1648 | 1380 | 0.84 | 1177 | 0.71 | |
| C30-50 × 1.6A | 50.8 | 1.6 | 152 | 3.0 | 298 | 30 | 260 | 250 | 0.96 | 163 | 0.63 | [32] |
| C30-50 × 1.6B | 50.8 | 1.6 | 152 | 3.0 | 298 | 30 | 280 | 250 | 0.89 | 163 | 0.58 | |
| C30-100 × 1.6A | 101.6 | 1.6 | 305 | 3.0 | 320 | 30 | 602 | 581 | 0.97 | 489 | 0.81 | |
| C30-100 × 1.6B | 101.6 | 1.6 | 305 | 3.0 | 320 | 30 | 609 | 593 | 0.97 | 489 | 0.80 | |
| A1 | 300.0 | 8.0 | 900 | 3.0 | 248 | 34 | 6134 | 6421 | 1.05 | 5047 | 0.82 | [43] |
| A2 | 300.0 | 10.0 | 900 | 3.0 | 242 | 34 | 7076 | 7524 | 1.06 | 5465 | 0.77 | |
| A3 | 300.0 | 12.0 | 900 | 3.0 | 249 | 34 | 8088 | 8611 | 1.06 | 6068 | 0.75 | |
| A6 | 300.0 | 12.0 | 900 | 3.0 | 249 | 38 | 8230 | 8797 | 1.07 | 6299 | 0.77 | |
| A7 | 300.0 | 8.0 | 900 | 3.0 | 248 | 41 | 6171 | 6704 | 1.09 | 5477 | 0.89 | |
| D2 | 325.0 | 10.0 | 975 | 3.0 | 542 | 37 | 11,032 | 11,937 | 1.08 | 10,222 | 0.93 | |
| D3 | 325.0 | 12.0 | 975 | 3.0 | 542 | 37 | 12,962 | 13,789 | 1.06 | 11,328 | 0.87 | |
| C-3-L-RS-1 | 159.0 | 2.9 | 477 | 3.0 | 384 | 37 | 1264 | 1337 | 1.06 | 1531 | 1.21 | [45] |
| C-3-L-RS-2 | 159.0 | 2.9 | 477 | 3.0 | 384 | 37 | 1322 | 1337 | 1.01 | 1531 | 1.16 | |
| C-3-H-RS-1 | 159.0 | 2.9 | 477 | 3.0 | 384 | 44 | 1349 | 1439 | 1.07 | 1661 | 1.23 | |
| C-3-H-RS-2 | 159.0 | 2.9 | 477 | 3.0 | 384 | 44 | 1316 | 1439 | 1.09 | 1661 | 1.26 | |
| C-4-L-RS-1 | 159.0 | 3.8 | 477 | 3.0 | 401 | 37 | 1627 | 1620 | 1.00 | 1774 | 1.09 | |
| C-4-L-RS-2 | 159.0 | 3.8 | 477 | 3.0 | 401 | 37 | 1624 | 1620 | 1.00 | 1774 | 1.09 | |
| C-5-L-RS-1 | 159.0 | 4.5 | 477 | 3.0 | 401 | 37 | 1713 | 1799 | 1.05 | 1941 | 1.13 | |
| C-5-L-RS-2 | 159.0 | 4.5 | 477 | 3.0 | 401 | 37 | 1630 | 1799 | 1.10 | 1941 | 1.19 | |
| C-3-L-DS-1 | 159.0 | 2.9 | 477 | 3.0 | 384 | 37 | 1310 | 1337 | 1.02 | 1531 | 1.17 | |
| C-3-L-DS-2 | 159.0 | 2.9 | 477 | 3.0 | 384 | 37 | 1291 | 1337 | 1.04 | 1531 | 1.19 | |
| C-3-H-DS-1 | 159.0 | 2.9 | 477 | 3.0 | 384 | 44 | 1514 | 1439 | 0.95 | 1661 | 1.10 | |
| C-3-H-DS-2 | 159.0 | 2.9 | 477 | 3.0 | 384 | 44 | 1552 | 1439 | 0.93 | 1661 | 1.07 | |
| C-4-L-DS-1 | 159.0 | 3.8 | 477 | 3.0 | 401 | 37 | 1598 | 1620 | 1.01 | 1774 | 1.11 | |
| C-4-L-DS-2 | 159.0 | 3.8 | 477 | 3.0 | 401 | 37 | 1612 | 1620 | 1.00 | 1774 | 1.10 | |
| C-5-L-DS-1 | 159.0 | 4.5 | 477 | 3.0 | 401 | 37 | 1725 | 1799 | 1.04 | 1941 | 1.13 | |
| C-5-L-DS-2 | 159.0 | 4.5 | 477 | 3.0 | 401 | 37 | 1739 | 1799 | 1.03 | 1941 | 1.12 | |
| C-3-L-SS-1 | 159.0 | 2.9 | 477 | 3.0 | 384 | 37 | 1366 | 1337 | 0.98 | 1531 | 1.12 | |
| C-3-L-SS-2 | 159.0 | 2.9 | 477 | 3.0 | 384 | 37 | 1333 | 1337 | 1.00 | 1531 | 1.15 | |
| C-3-H-SS-1 | 159.0 | 2.9 | 477 | 3.0 | 384 | 44 | 1466 | 1439 | 0.98 | 1661 | 1.13 | |
| C-3-H-SS-2 | 159.0 | 2.9 | 477 | 3.0 | 384 | 44 | 1452 | 1439 | 0.99 | 1661 | 1.14 | |
| C-4-L-SS-1 | 159.0 | 3.8 | 477 | 3.0 | 401 | 37 | 1642 | 1620 | 0.99 | 1774 | 1.08 | |
| C-4-L-SS-2 | 159.0 | 3.8 | 477 | 3.0 | 401 | 37 | 1648 | 1620 | 0.98 | 1774 | 1.08 | |
| C-5-L-SS-1 | 159.0 | 4.5 | 477 | 3.0 | 401 | 37 | 1746 | 1799 | 1.03 | 1941 | 1.11 | |
| C-5-L-SS-2 | 159.0 | 4.5 | 477 | 3.0 | 401 | 37 | 1715 | 1799 | 1.05 | 1941 | 1.13 | |
| S50-C | 50.9 | 3.1 | 150 | 2.9 | 228 | 36 | 235 | 241 | 1.03 | 205 | 0.87 | [41] |
| S101-C | 101.9 | 2.8 | 400 | 3.9 | 225 | 36 | 570 | 581 | 1.02 | 578 | 1.01 | |
| S114-C | 114.1 | 2.8 | 400 | 3.5 | 280 | 36 | 766 | 762 | 0.99 | 764 | 1.00 | |
| S165-C | 168.4 | 3.2 | 400 | 2.4 | 281 | 36 | 1449 | 1391 | 0.96 | 1506 | 1.04 | |
| 50x1.6-F | 49.6 | 1.5 | 150 | 3.0 | 376 | 42 | 209 | 208 | 1.00 | 198 | 0.95 | [42] |
| 50x3-F | 50.9 | 3.1 | 150 | 2.9 | 229 | 42 | 244 | 256 | 1.05 | 217 | 0.89 | |
| 76x1.6-F | 76.2 | 1.7 | 230 | 3.0 | 398 | 42 | 388 | 410 | 1.06 | 411 | 1.06 | |
| 89x3-F | 89.2 | 3.2 | 270 | 3.0 | 259 | 42 | 548 | 592 | 1.08 | 569 | 1.04 | |
| 101x1.6-F | 101.8 | 1.7 | 300 | 2.9 | 353 | 42 | 617 | 570 | 0.92 | 621 | 1.01 | |
| 101x3-F | 101.9 | 2.8 | 300 | 2.9 | 226 | 42 | 610 | 612 | 1.00 | 622 | 1.02 | |
| 114x3-F | 114.1 | 2.8 | 350 | 3.1 | 281 | 42 | 831 | 799 | 0.96 | 824 | 0.99 | |
| 152x1.6-F | 152.6 | 1.6 | 450 | 2.9 | 314 | 42 | 1050 | 945 | 0.90 | 1138 | 1.08 | |
| 203x2-F | 202.7 | 2.0 | 600 | 3.0 | 304 | 42 | 1787 | 1576 | 0.88 | 1955 | 1.09 | |
| C-S-N | 120.0 | 1.8 | 360 | 3.0 | 286 | 54 | 823 | 760 | 0.92 | 890 | 1.08 | [35] |
| C-S-C1 | 120.0 | 1.8 | 360 | 3.0 | 286 | 51 | 813 | 732 | 0.90 | 856 | 1.05 | |
| C-S-C2 | 120.0 | 1.8 | 360 | 3.0 | 286 | 49 | 802 | 714 | 0.89 | 837 | 1.04 | |
| C-S-C3 | 120.0 | 1.8 | 360 | 3.0 | 286 | 48 | 774 | 705 | 0.91 | 826 | 1.07 | |
| C-S-F1 | 120.0 | 1.8 | 360 | 3.0 | 286 | 50 | 806 | 723 | 0.90 | 850 | 1.05 | |
| C-S-F2 | 120.0 | 1.8 | 360 | 3.0 | 286 | 48 | 768 | 705 | 0.92 | 826 | 1.08 | |
| C-S-F3 | 120.0 | 1.8 | 360 | 3.0 | 286 | 47 | 777 | 696 | 0.90 | 815 | 1.05 | |
| C-100S | 103.0 | 1.7 | 306 | 3.0 | 213 | 50 | 552 | 503 | 0.91 | 588 | 1.07 | [44] |
| C-150S | 153.0 | 2.1 | 456 | 3.0 | 209 | 50 | 1138 | 1020 | 0.90 | 1235 | 1.09 | |
| C-200S | 203.0 | 2.1 | 608 | 3.0 | 209 | 50 | 1868 | 1639 | 0.88 | 2044 | 1.09 | |
| C5 | 100.0 | 2.0 | 300 | 3.0 | 324 | 39 | 591 | 530 | 0.90 | 595 | 1.01 | [34] |
| D73-C50 | 72.8 | 2.9 | 215 | 3.0 | 258 | 50 | 375 | 391 | 1.04 | 421 | 1.12 | [63] |
| D73-C60 | 72.8 | 2.8 | 216 | 3.0 | 258 | 64 | 455 | 432 | 0.95 | 473 | 1.04 | |
| D89-C60 | 89.3 | 3.1 | 266 | 3.0 | 321 | 64 | 685 | 688 | 1.00 | 755 | 1.10 | |
| C-3–0.9–3.0 | 63.0 | 0.9 | 189 | 3.0 | 350 | 19 | 135 | 152 | 1.13 | 149 | 1.10 | [36] |
| C-3–1.0–3.0 | 63.0 | 1.0 | 189 | 3.0 | 423 | 19 | 192 | 187 | 0.97 | 163 | 0.85 | |
| C-3–1.2–3.0 | 63.0 | 1.2 | 189 | 3.0 | 330 | 19 | 163 | 182 | 1.12 | 202 | 1.24 | |
| C-4–0.9–3.0 | 63.0 | 0.9 | 189 | 3.0 | 350 | 22 | 263 | 250 | 0.95 | 159 | 0.60 | |
| C-4–1.0–3.0 | 63.0 | 1.0 | 189 | 3.0 | 423 | 22 | 184 | 193 | 1.05 | 172 | 0.93 | |
| C-3–0.9–3.5 | 63.0 | 0.9 | 221 | 3.5 | 350 | 19 | 204 | 215 | 1.05 | 149 | 0.73 | |
| C-3–1.0–3.5 | 63.0 | 1.0 | 221 | 3.5 | 423 | 19 | 252 | 264 | 1.05 | 163 | 0.65 | |
| C-3–1.2–3.5 | 63.0 | 1.2 | 221 | 3.5 | 330 | 19 | 326 | 335 | 1.03 | 202 | 0.62 | |
| C-4–0.9–3.5 | 63.0 | 0.9 | 221 | 3.5 | 350 | 22 | 125 | 135 | 1.08 | 159 | 1.27 | |

(continued on next page)

**Table 1** (*continued*)

| Specimen | $b(b=h)$ (mm) | $t$ (mm) | $L$ (mm) | $L/b$ | $\sigma_{0.2}$ (MPa) | $f_c'$ (MPa) | $P_{u,exp}$ (kN) | $P_{u,num}$ (kN) | $\frac{P_{u,num}}{P_{u,exp}}$ | $P_{u,Lin}$ (kN) | $\frac{P_{u,Lin}}{P_{u,exp}}$ | Ref. |
|---|---|---|---|---|---|---|---|---|---|---|---|---|
| C-4–1.0–3.5 | 63.0 | 1.0 | 221 | 3.5 | 423 | 22 | 203 | 199 | 0.98 | 172 | 0.85 | |
| C-4–1.2–3.5 | 63.0 | 1.2 | 221 | 3.5 | 350 | 22 | 272 | 295 | 1.08 | 212 | 0.78 | |
| C-3–1.0–4.0 | 63.0 | 1.0 | 252 | 4.0 | 423 | 19 | 233 | 240 | 1.03 | 163 | 0.70 | |
| C-3–1.2–4.0 | 63.0 | 1.2 | 252 | 4.0 | 330 | 19 | 286 | 293 | 1.02 | 202 | 0.71 | |
| C-4–0.9–4.0 | 63.0 | 0.9 | 252 | 4.0 | 350 | 22 | 135 | 137 | 1.01 | 159 | 1.18 | |
| C-4–1.0–4.0 | 63.0 | 1.0 | 252 | 4.0 | 423 | 22 | 250 | 276 | 1.10 | 172 | 0.69 | |
| C-4–1.2–4.0 | 63.0 | 1.2 | 252 | 4.0 | 338 | 22 | 272 | 281 | 1.03 | 212 | 0.78 | |
| | | Mean | | | | | | | 1.00 | | 0.99 | |
| | | Standard Deviation (SD) | | | | | | | 0.07 | | 0.18 | |
| | | Coefficient of Variance (CoV) | | | | | | | 0.07 | | 0.18 | |

**Table 2**
Validation of the accuracy of the unified model for rectangular CFSST columns.

| Specimen | $b$ (mm) | $h$ (mm) | $t$ (mm) | $L$ (mm) | $L/b$ | $f_c'$ (MPa) | $\sigma_{0.2}$ (MPa) | $P_{u,exp}$ (kN) | $P_{u,num}$ (kN) | $\frac{P_{u,num}}{P_{u,exp}}$ | $P_{u,Lin}$ (kN) | $\frac{P_{u,Lin}}{P_{u,exp}}$ | Ref |
|---|---|---|---|---|---|---|---|---|---|---|---|---|---|
| SHS1C40 | 150.5 | 150.5 | 5.8 | 450 | 3.0 | 47 | 497 | 2768 | 2729 | 0.99 | 2594 | 0.94 | [30] |
| SHS1C60 | 150.5 | 150.5 | 5.8 | 450 | 3.0 | 62 | 497 | 2972 | 2899 | 0.98 | 2882 | 0.97 | |
| SHS1C80 | 150.5 | 150.5 | 5.8 | 450 | 3.0 | 84 | 497 | 3020 | 3199 | 1.06 | 3295 | 1.09 | |
| S30-50 × 2A | 51.0 | 51.0 | 1.8 | 150 | 2.9 | 35 | 353 | 268 | 214 | 0.80 | 205 | 0.76 | [32] |
| S30-50 × 2B | 51.0 | 51.0 | 1.8 | 150 | 2.9 | 35 | 353 | 274 | 214 | 0.78 | 205 | 0.75 | |
| S20-100 × 3A | 100.0 | 100.0 | 2.9 | 300 | 3.0 | 22 | 358 | 705 | 649 | 0.92 | 595 | 0.84 | |
| S20-100 × 3B | 100.0 | 100.0 | 2.9 | 300 | 3.0 | 22 | 358 | 716 | 649 | 0.91 | 595 | 0.83 | |
| S30-100 × 3A | 100.0 | 100.0 | 2.9 | 300 | 3.0 | 35 | 358 | 765 | 719 | 0.94 | 709 | 0.93 | |
| S30-100 × 3B | 100.0 | 100.0 | 2.9 | 300 | 3.0 | 35 | 358 | 757 | 728 | 0.96 | 709 | 0.94 | |
| S20-100 × 5A | 101.0 | 101.0 | 5.1 | 300 | 3.0 | 22 | 435 | 1437 | 1452 | 1.01 | 1020 | 0.71 | |
| S20-100 × 5B | 101.0 | 101.0 | 5.1 | 300 | 3.0 | 22 | 435 | 1449 | 1452 | 1.00 | 1020 | 0.70 | |
| S30-100 × 5A | 101.0 | 101.0 | 5.1 | 300 | 3.0 | 35 | 435 | 1474 | 1478 | 1.00 | 1136 | 0.77 | |
| S30-100 × 5B | 101.0 | 101.0 | 5.1 | 300 | 3.0 | 35 | 435 | 1490 | 1478 | 0.99 | 1136 | 0.76 | |
| S20-150 × 3A | 152.0 | 152.0 | 2.9 | 450 | 3.0 | 22 | 268 | 1035 | 893 | 0.86 | 926 | 0.89 | |
| S20-150 × 3B | 152.0 | 152.0 | 2.9 | 450 | 3.0 | 22 | 268 | 1062 | 893 | 0.84 | 926 | 0.87 | |
| S30-150 × 3A | 152.0 | 152.0 | 2.9 | 450 | 3.0 | 35 | 268 | 1074 | 1126 | 1.05 | 1207 | 1.12 | |
| S30-150 × 3B | 152.0 | 152.0 | 2.9 | 450 | 3.0 | 35 | 268 | 1209 | 1126 | 0.93 | 1207 | 1.00 | |
| S20-150 × 5B | 150.0 | 150.0 | 4.8 | 450 | 3.0 | 22 | 340 | 1935 | 2144 | 1.11 | 1380 | 0.71 | |
| S30-150 × 5A | 150.0 | 150.0 | 4.8 | 450 | 3.0 | 35 | 340 | 2048 | 1877 | 0.92 | 1634 | 0.80 | |
| S30-150 × 5B | 150.0 | 150.0 | 4.8 | 450 | 3.0 | 35 | 340 | 1976 | 1652 | 0.84 | 1634 | 0.83 | |
| SHS 100 × 100 × 5 – C30 | 100.6 | 100 | 5.0 | 300 | 3.0 | 30 | 458 | 1410 | 1373 | 0.97 | 1121 | 0.80 | [31] |
| SHS 100 × 100 × 5 – C60 | 99.9 | 101 | 4.9 | 300 | 3.0 | 53 | 458 | 1488 | 1422 | 0.96 | 1291 | 0.87 | |
| SHS 100 × 100 × 5 – C100 | 99.9 | 101 | 4.9 | 300 | 3.0 | 74 | 458 | 1559 | 1532 | 0.98 | 1467 | 0.94 | |
| 304-t8C50 | 295.5 | 296 | 7.8 | 840 | 2.8 | 41 | 293 | 6290 | 5457 | 0.87 | 5854 | 0.93 | [46] |
| 304-t10C50 | 299.7 | 300 | 9.9 | 840 | 2.8 | 41 | 287 | 7113 | 6217 | 0.87 | 6517 | 0.92 | |
| 304-t12C50 | 303.7 | 304 | 11.9 | 840 | 2.8 | 41 | 301 | 7924 | 6963 | 0.88 | 7415 | 0.94 | |
| 304-t8C70 | 295.5 | 296 | 7.8 | 840 | 2.8 | 61 | 293 | 6743 | 6690 | 0.99 | 7442 | 1.10 | |
| 304-t10C70 | 299.7 | 300 | 9.9 | 840 | 2.8 | 61 | 287 | 7947 | 7356 | 0.93 | 8125 | 1.02 | |
| 304-t12C70 | 303.7 | 304 | 11.9 | 840 | 2.8 | 61 | 301 | 8575 | 8016 | 0.93 | 9025 | 1.05 | |
| 304-t8C80 | 295.5 | 296 | 7.8 | 840 | 2.8 | 70 | 293 | 7436 | 7259 | 0.98 | 8144 | 1.10 | |
| 304-t10C80 | 299.7 | 300 | 9.9 | 840 | 2.8 | 70 | 287 | 8430 | 7890 | 0.94 | 8836 | 1.05 | |
| 304-t12C80 | 303.7 | 304 | 11.9 | 840 | 2.8 | 70 | 301 | 9257 | 8520 | 0.92 | 9725 | 1.05 | |
| 2205-t8C50 | 295.5 | 296 | 7.9 | 840 | 2.8 | 41 | 634 | 8771 | 9430 | 1.08 | 8826 | 1.01 | |
| 2205-t10C50 | 299.7 | 300 | 9.8 | 840 | 2.8 | 41 | 590 | 10,111 | 10,917 | 1.08 | 9831 | 0.97 | |
| 2205-t12C50 | 303.7 | 304 | 12.5 | 840 | 2.8 | 41 | 576 | 12,472 | 13,337 | 1.07 | 11,565 | 0.93 | |
| 2205-t8C70 | 295.5 | 296 | 7.9 | 840 | 2.8 | 61 | 634 | 9686 | 10,196 | 1.05 | 10,423 | 1.08 | |
| 2205-t10C70 | 299.7 | 300 | 9.8 | 840 | 2.8 | 61 | 590 | 10,820 | 11,271 | 1.04 | 11,522 | 1.06 | |
| 2205-t12C70 | 303.7 | 304 | 12.5 | 840 | 2.8 | 61 | 576 | 12,560 | 13,760 | 1.10 | 13,114 | 1.04 | |
| 2205-t8C80 | 295.5 | 296 | 7.9 | 840 | 2.8 | 70 | 634 | 9962 | 10,699 | 1.07 | 11,120 | 1.12 | |
| 2205-t10C80 | 299.7 | 300 | 9.8 | 840 | 2.8 | 70 | 590 | 11,728 | 11,660 | 0.99 | 12,208 | 1.04 | |
| 2205-t12C80 | 303.7 | 304 | 12.5 | 840 | 2.8 | 70 | 576 | 13,272 | 13,891 | 1.05 | 13,827 | 1.04 | |
| S200635 | 60.0 | 60 | 1.0 | 180 | 3.0 | 19 | 258 | 131 | 124 | 0.95 | 124 | 0.95 | [37] |
| S200640 | 60.0 | 60 | 1.0 | 180 | 3.0 | 19 | 258 | 126 | 124 | 0.98 | 124 | 0.98 | |
| S200830 | 80.0 | 80 | 1.0 | 240 | 3.0 | 19 | 258 | 190 | 193 | 1.02 | 197 | 1.04 | |
| S200835 | 80.0 | 80 | 1.0 | 240 | 3.0 | 19 | 258 | 182 | 193 | 1.06 | 197 | 1.08 | |
| S2001030 | 100.0 | 100 | 1.0 | 300 | 3.0 | 19 | 258 | 258 | 274 | 1.06 | 284 | 1.10 | |
| S300840 | 80.0 | 80 | 1.0 | 300 | 3.8 | 25 | 258 | 211 | 227 | 1.08 | 234 | 1.11 | |
| S-3-L-RS-2 | 160.0 | 160.0 | 2.9 | 480 | 3.0 | 37 | 446 | 1534 | 1612 | 1.05 | 1690 | 1.10 | [45] |
| S-4-L-RS-1 | 160.0 | 160.0 | 3.9 | 480 | 3.0 | 37 | 415 | 2040 | 1832 | 0.90 | 1874 | 0.92 | |
| S-4-L-RS-2 | 160.0 | 160.0 | 3.9 | 480 | 3.0 | 37 | 415 | 1931 | 1832 | 0.95 | 1874 | 0.97 | |
| S-5-L-RS-1 | 160.0 | 160.0 | 4.8 | 480 | 3.0 | 37 | 432 | 2125 | 2167 | 1.02 | 2124 | 1.00 | |
| S-5-L-RS-2 | 160.0 | 160.0 | 4.8 | 480 | 3.0 | 37 | 432 | 2012 | 2167 | 1.08 | 2124 | 1.06 | |
| S-3-L-DS-1 | 160.0 | 160.0 | 2.9 | 480 | 3.0 | 37 | 446 | 1543 | 1612 | 1.04 | 1690 | 1.10 | |
| S-3-L-DS-2 | 160.0 | 160.0 | 2.9 | 480 | 3.0 | 37 | 446 | 1590 | 1612 | 1.01 | 1690 | 1.06 | |
| S-3-H-DS-1 | 160.0 | 160.0 | 2.9 | 480 | 3.0 | 44 | 446 | 1769 | 1748 | 0.99 | 1858 | 1.05 | |
| S-3-H-DS-2 | 160.0 | 160.0 | 2.9 | 480 | 3.0 | 44 | 446 | 1914 | 1748 | 0.91 | 1858 | 0.97 | |
| S-4-L-DS-1 | 160.0 | 160.0 | 3.9 | 480 | 3.0 | 37 | 415 | 1955 | 1832 | 0.94 | 1874 | 0.96 | |

(*continued on next page*)

**Table 2** (*continued*)

| Specimen | $b$ (mm) | $h$ (mm) | $t$ (mm) | $L$ (mm) | $L/b$ | $f_c$ (MPa) | $\sigma_{0.2}$ (MPa) | $P_{u,exp}$ (kN) | $P_{u,num}$ (kN) | $\frac{P_{u,num}}{P_{u,exp}}$ | $P_{u,Lin}$ (kN) | $\frac{P_{u,Lin}}{P_{u,exp}}$ | Ref |
|---|---|---|---|---|---|---|---|---|---|---|---|---|---|
| S-4-L-DS-2 | 160.0 | 160.0 | 3.9 | 480 | 3.0 | 37 | 415 | 1897 | 1832 | 0.97 | 1874 | 0.99 | |
| S-5-L-DS-1 | 160.0 | 160.0 | 4.8 | 480 | 3.0 | 37 | 432 | 2152 | 2167 | 1.01 | 2124 | 0.99 | |
| S-5-L-DS-2 | 160.0 | 160.0 | 4.8 | 480 | 3.0 | 37 | 432 | 2141 | 2167 | 1.01 | 2124 | 0.99 | |
| S-3-L-SS-1 | 160.0 | 160.0 | 2.9 | 480 | 3.0 | 37 | 446 | 1724 | 1612 | 0.94 | 1690 | 0.98 | |
| S-3-L-SS-2 | 160.0 | 160.0 | 2.9 | 480 | 3.0 | 37 | 446 | 1780 | 1612 | 0.91 | 1690 | 0.95 | |
| S-3-H-SS-1 | 160.0 | 160.0 | 2.9 | 480 | 3.0 | 44 | 446 | 1690 | 1748 | 1.03 | 1858 | 1.10 | |
| S-3-H-SS-2 | 160.0 | 160.0 | 2.9 | 480 | 3.0 | 44 | 446 | 1765 | 1748 | 0.99 | 1858 | 1.05 | |
| S-4-L-SS-1 | 160.0 | 160.0 | 3.9 | 480 | 3.0 | 37 | 415 | 2007 | 1832 | 0.91 | 1874 | 0.93 | |
| S-4-L-SS-2 | 160.0 | 160.0 | 3.9 | 480 | 3.0 | 37 | 415 | 1947 | 1832 | 0.94 | 1874 | 0.96 | |
| S-5-L-SS-1 | 160.0 | 160.0 | 4.8 | 480 | 3.0 | 37 | 432 | 2215 | 2167 | 0.98 | 2124 | 0.96 | |
| S-5-L-SS-2 | 160.0 | 160.0 | 4.8 | 480 | 3.0 | 37 | 432 | 2197 | 2167 | 0.99 | 2124 | 0.97 | |
| A100 | 98.8 | 98.8 | 3.1 | 400 | 4.0 | 37 | 266 | 698 | 628 | 0.90 | 634 | 0.91 | [49] |
| A250 | 248.8 | 248.8 | 3.1 | 850 | 3.4 | 37 | 266 | 2709 | 2597 | 0.96 | 2992 | 1.10 | |
| D100 | 99.5 | 99.5 | 3.1 | 400 | 4.0 | 37 | 511 | 1039 | 989 | 0.95 | 933 | 0.90 | |
| D250 | 249.5 | 249.5 | 3.1 | 850 | 3.4 | 37 | 511 | 3186 | 3374 | 1.06 | 3736 | 1.17 | |
| 60 × 40 × 4C40 | 59.9 | 40.1 | 3.8 | 179 | 3.0 | 43 | 479 | 478 | 525 | 1.10 | 410 | 0.86 | [91] |
| 60 × 40 × 4C40R | 59.8 | 40.1 | 3.8 | 179 | 3.0 | 43 | 479 | 481 | 525 | 1.09 | 410 | 0.85 | |
| 60 × 40 × 4C80 | 59.9 | 40.1 | 3.8 | 179 | 3.0 | 81 | 479 | 531 | 549 | 1.03 | 474 | 0.89 | |
| 60 × 40 × 4C120 | 59.8 | 40.1 | 3.8 | 179 | 3.0 | 115 | 479 | 585 | 563 | 0.96 | 529 | 0.90 | |
| 60 × 60 × 3C40 | 60.3 | 60.1 | 2.8 | 179 | 3.0 | 43 | 449 | 484 | 473 | 0.98 | 419 | 0.87 | |
| 60 × 60 × 3C80 | 60.2 | 60.1 | 2.8 | 179 | 3.0 | 81 | 449 | 594 | 535 | 0.90 | 530 | 0.89 | |
| 80 × 60 × 4C40 | 80.1 | 59.9 | 3.7 | 240 | 3.0 | 43 | 451 | 712 | 713 | 1.00 | 605 | 0.85 | |
| 80 × 60 × 4C80 | 80.3 | 59.9 | 3.7 | 240 | 3.0 | 81 | 451 | 878 | 778 | 0.89 | 755 | 0.86 | |
| 80 × 60 × 4C120 | 80.2 | 59.9 | 3.7 | 240 | 3.0 | 115 | 451 | 999 | 881 | 0.88 | 878 | 0.88 | |
| 80 × 60 × 4C120R | 80.2 | 59.9 | 3.7 | 240 | 3.0 | 115 | 451 | 976 | 881 | 0.90 | 883 | 0.90 | |
| 100 × 40 × 2C40 | 99.7 | 40.2 | 1.9 | 300 | 3.0 | 43 | 420 | 398 | 380 | 0.95 | 367 | 0.92 | |
| 100 × 40 × 2C120 | 99.7 | 40.2 | 1.9 | 300 | 3.0 | 115 | 420 | 674 | 600 | 0.89 | 619 | 0.92 | |
| 120 × 80 × 3C40 | 119.9 | 79.9 | 2.8 | 360 | 3.0 | 43 | 381 | 870 | 784 | 0.90 | 780 | 0.90 | |
| 120 × 80 × 3C80 | 120.0 | 79.9 | 2.8 | 360 | 3.0 | 81 | 381 | 1255 | 1069 | 0.85 | 1105 | 0.88 | |
| 120 × 80 × 3C120 | 120.0 | 79.9 | 2.8 | 360 | 3.0 | 115 | 381 | 1610 | 1333 | 0.83 | 1397 | 0.87 | |
| Mean | | | | | | | | | | 0.97 | | 0.95 | |
| SD | | | | | | | | | | 0.07 | | 0.11 | |
| CoV | | | | | | | | | | 0.08 | | 0.11 | |

**Table 3**
Validation of the accuracy of the unified model for round-ended CFST columns.

| Specimen | $b$ (mm) | $h$ (mm) | $t$ (mm) | $L$ (mm) | $L/b$ | $\sigma_{0.2}$ (MPa) | $f_c$ (MPa) | $P_{u,exp}$ (kN) | $P_{u,num}$ (kN) | $\frac{P_{u,num}}{P_{u,exp}}$ | $P_{u,Lin}$ (kN) | $\frac{P_{u,Lin}}{P_{u,exp}}$ | Ref |
|---|---|---|---|---|---|---|---|---|---|---|---|---|---|
| WST1-A | 299 | 252 | 3.75 | 750 | 2.5 | 328 | 34 | 3429 | 3504 | 1.02 | 3647 | 1.06 | [92] |
| WST1-B | 302 | 249 | 3.75 | 750 | 2.5 | 328 | 34 | 3328 | 3486 | 1.05 | 3645 | 1.10 | |
| WST2-A | 299 | 255 | 5.84 | 750 | 2.5 | 300 | 34 | 4162 | 3915 | 0.94 | 4222 | 1.01 | |
| WST2-B | 300 | 251 | 5.8 | 750 | 2.5 | 300 | 34 | 4168 | 3859 | 0.93 | 4170 | 1.00 | |
| WST3-A | 350 | 255 | 3.72 | 900 | 2.6 | 328 | 34 | 3929 | 3924 | 1.00 | 4210 | 1.07 | |
| WST3-B | 351 | 252 | 3.76 | 900 | 2.6 | 328 | 34 | 4158 | 3896 | 0.94 | 4200 | 1.01 | |
| WST4-A | 352 | 251 | 5.9 | 900 | 2.6 | 300 | 34 | 4492 | 4320 | 0.96 | 4792 | 1.07 | |
| WST4-B | 349 | 251 | 5.92 | 900 | 2.6 | 300 | 43 | 5530 | 4950 | 0.90 | 5374 | 0.97 | |
| WST5-A | 394 | 260 | 3.79 | 1000 | 2.5 | 328 | 43 | 5620 | 5111 | 0.91 | 5497 | 0.98 | |
| WST5-B | 396 | 264 | 3.8 | 1000 | 2.5 | 328 | 43 | 5500 | 5217 | 0.95 | 5594 | 1.02 | |
| WST6-A | 405 | 197 | 3.75 | 800 | 2.0 | 311 | 33 | 3240 | 3359 | 1.04 | 3846 | 1.19 | |
| WST7-A | 608 | 186 | 3.75 | 1200 | 2.0 | 311 | 33 | 4826 | 4834 | 1.00 | 5451 | 1.13 | |
| WST7-B | 605 | 194 | 3.77 | 1200 | 2.0 | 311 | 33 | 4944 | 4961 | 1.00 | 5599 | 1.13 | |
| WST8-A | 805 | 190 | 3.74 | 1600 | 2.0 | 311 | 33 | 6521 | 6504 | 1.00 | 7263 | 1.11 | |
| WST8-B | 806 | 191 | 3.67 | 1600 | 2.0 | 311 | 33 | 6493 | 6502 | 1.00 | 7254 | 1.12 | |
| WST9-A | 405 | 198 | 3.75 | 800 | 2.0 | 311 | 49 | 4203 | 4387 | 1.04 | 4922 | 1.17 | |
| WST9-B | 405 | 198 | 3.7 | 800 | 2.0 | 311 | 49 | 4180 | 4373 | 1.05 | 4906 | 1.17 | |
| WST10-A | 610 | 196 | 3.8 | 1200 | 2.0 | 311 | 49 | 7201 | 6618 | 0.92 | 7321 | 1.02 | |
| WST10-B | 606 | 189 | 3.77 | 1200 | 2.0 | 311 | 49 | 6905 | 6384 | 0.92 | 7060 | 1.02 | |
| WST11-A | 805 | 190 | 3.68 | 1600 | 2.0 | 311 | 49 | 9065 | 8526 | 0.94 | 9336 | 1.03 | |
| WST11-B | 805 | 194 | 3.8 | 1600 | 2.0 | 311 | 49 | 8799 | 8722 | 0.99 | 9561 | 1.09 | |
| RCFST-1 | 168.5 | 117 | 2.86 | 540 | 3.2 | 325 | 32 | 925 | 1030 | 1.11 | 1093 | 1.18 | [12] |
| RCFST-2 | 229 | 118 | 2.86 | 722 | 3.2 | 325 | 32 | 1215 | 1288 | 1.06 | 1435 | 1.18 | |
| RCFST-4 | 237.5 | 156.5 | 2.86 | 720 | 3.0 | 325 | 32 | 1658 | 1696 | 1.02 | 1825 | 1.10 | |
| RCFST-5 | 317 | 158.5 | 2.86 | 962 | 3.0 | 325 | 32 | 2091 | 2117 | 1.01 | 2393 | 1.14 | |
| RND_30_00 | 120 | 50 | 2 | 300 | 2.5 | 307 | 41 | 385 | 400 | 1.04 | 420 | 1.09 | [93] |
| Mean | | | | | | | | | | 0.99 | | 1.08 | |
| SD | | | | | | | | | | 0.06 | | 0.07 | |
| CoV | | | | | | | | | | 0.06 | | 0.06 | |

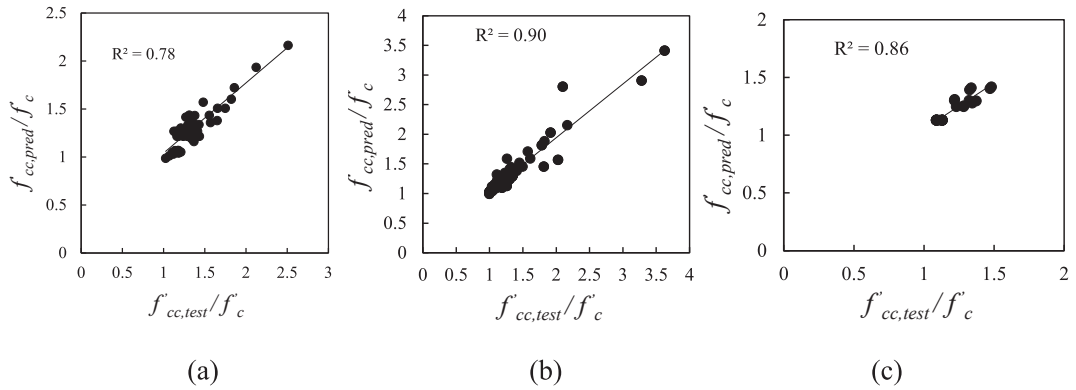


**Fig. 4.** Accuracy of the proposed formulas for $f'_{cc}/f'_c$: (a) circular, (b) rectangular and (c) round-ended cross-sections.

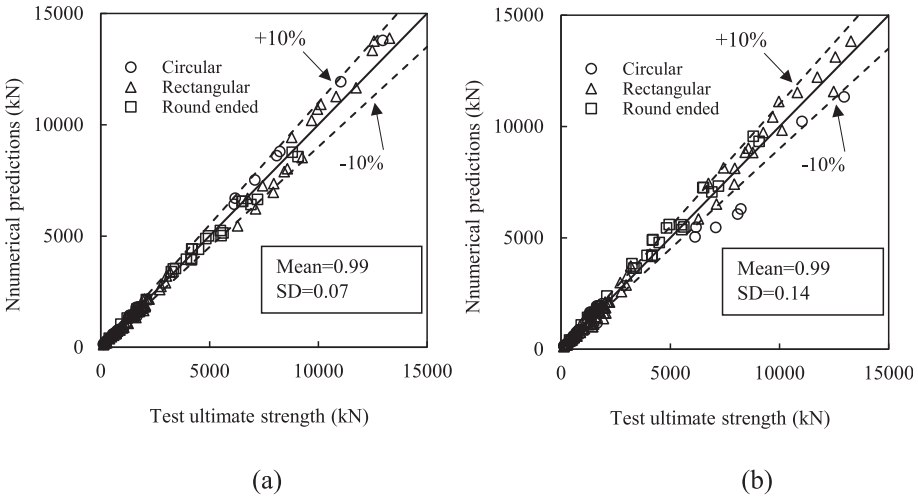


**Fig. 5.** Comparison of the predicted and test ultimate strength of all columns (a) unified model proposed in this study (b) unified model proposed by Lin et al. [72].

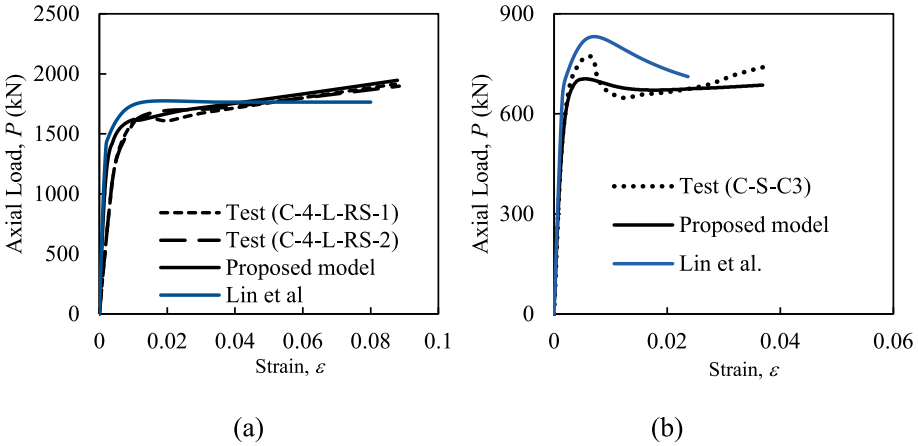


**Fig. 6.** Test vs numerical predictions of $P-\varepsilon$ curves of circular CFSST columns.

$$\sigma_c = \begin{cases} \dfrac{f'_{cc}(\varepsilon_c/\varepsilon'_{cc})\lambda}{(\varepsilon_c/\varepsilon'_{cc})^{\lambda}+\lambda-1} & \text{for } 0 \leqslant \varepsilon_c \leqslant \varepsilon'_{cc} \\ f'_{cc} - \dfrac{f'_{cc}-f_{cr}}{1+\left(\dfrac{\varepsilon_c-\varepsilon'_{cc}}{\varepsilon_{ci}-\varepsilon'_{cc}}\right)^{-2}} & \text{for } \varepsilon_c > \varepsilon'_{cc} \end{cases} \tag{40}$$

where $\varepsilon_c$ is the longitudinal strain at longitudinal stress $\sigma_c$; $f'_{cc}$ and $\varepsilon'_{cc}$ are the compressive strength of the confined concrete and its associated strain, respectively; $f_{cr}$ is the residual strength of concrete and $\varepsilon_{ci}$ represents the inflection strain; $\lambda$ is given by

$$\lambda = \frac{E_c\varepsilon'_{cc}}{E_c\varepsilon'_{cc} - f'_{cc}} \tag{41}$$

in which $E_c$ is the elastic moduli of concrete, calculated as $E_c = 4400\sqrt{\gamma_c f'_c}$ in MPa. The reduction factor $\gamma_c$ was provided by Liang [69] for taking into account the effect of the column size, calculated as $\gamma_c =$

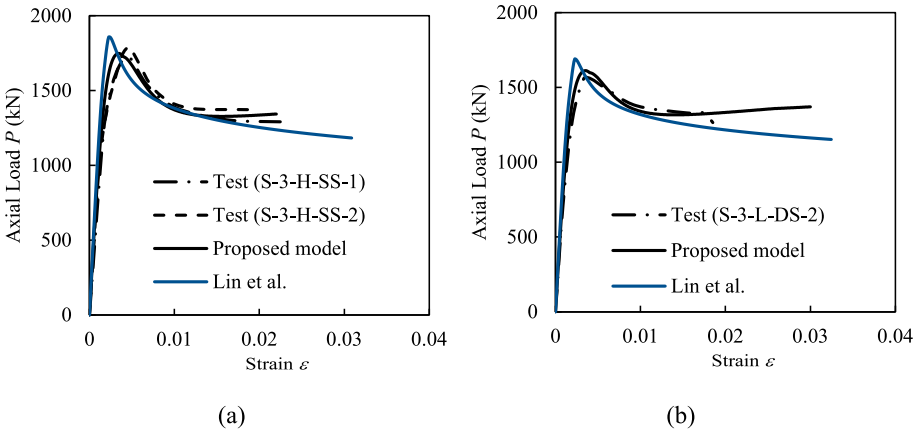


**Fig. 7.** Test vs numerical predictions of $P-\varepsilon$ curves of rectangular and square CFSST columns.

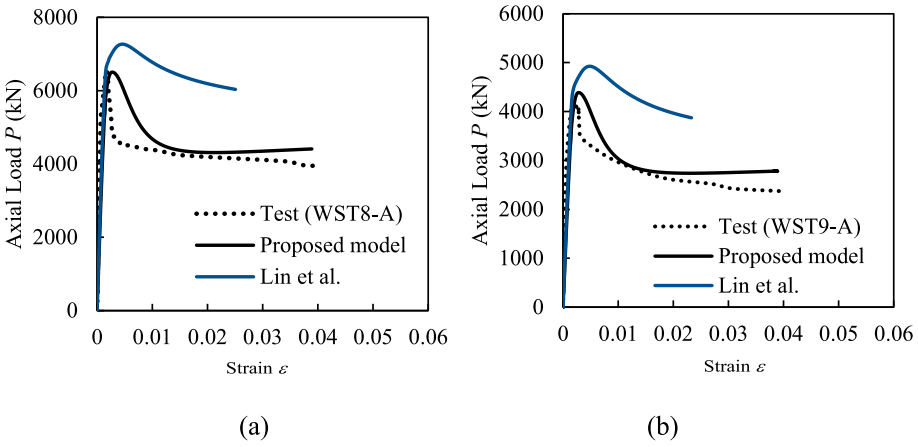


**Fig. 8.** Test vs numerical predictions of $P-\varepsilon$ curves of round-ended CFST columns.

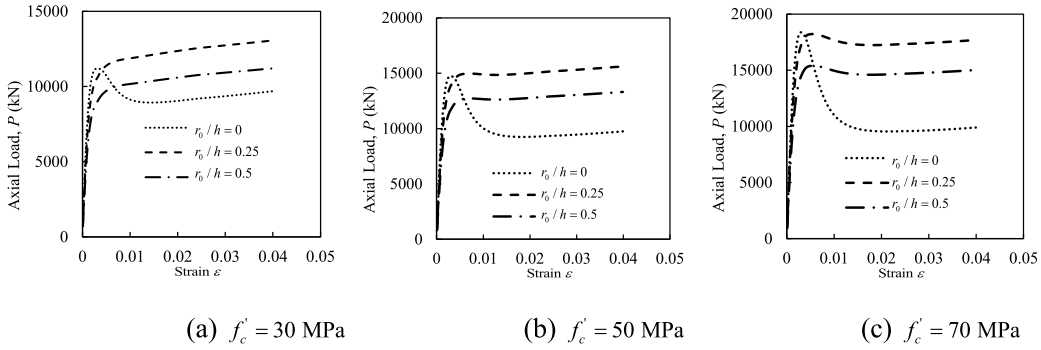


**Fig. 9.** Sensitivity of strength of concrete on the $P-\varepsilon$ curves for varying $r_0/h$ ratio.

1.85 $D_c^{-0.135} \geqslant 0.85$, where $D_c$ is the diameter of the core concrete ($D_c = 2R_e$).

The confinement effects are different for various shapes in CFSST columns. Due to the confinement, the compressive strength of confined concrete of CFSST columns is higher compared to unconfined concrete compressive strength, as can be seen from Fig. 3. The concrete compressive strength of the confined concrete ($f'_{cc}$) of the tested CFSST columns were calculated by subtracting the axial capacity of the stainless-steel tube from the ultimate axial load of the CFSST column. If the tested column had an obvious strain-softening branch, the ultimate strength was taken as the maximum load from their stress–strain curves. However, if the tested column had no obvious strain-softening branch, the ultimate load was taken as the axial load of the column at 1% strain based on the definition of the maximum concrete compressive strain. Based on the test data reported in Tables 1 to 3, $f'_{cc}/f'_c$ for all the tested columns were plotted and regression analysis was performed to proposed new formulas to calculate $f'_{cc}/f'_c$ for various cross-sections as

$$\frac{f'_{cc}}{f'_c} = \begin{cases} 0.44\xi + 0.9 \text{ (circular shape)} \\ 0.0612 \times \xi^2 + 0.1177 \times \xi + 0.9359 \text{ (rectangular and square shapes)} \end{cases} \quad (42)$$

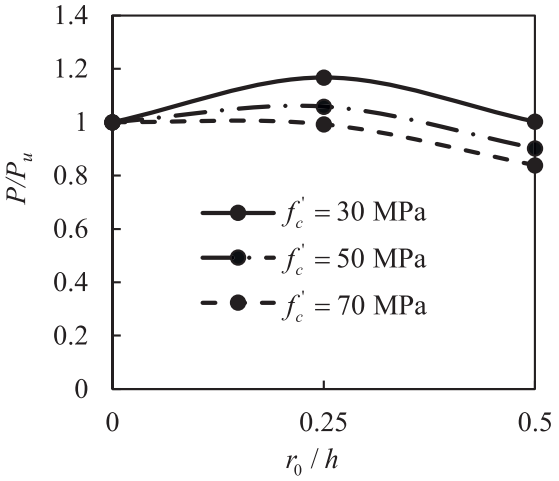


**Fig. 10.** Sensitivity of $r_0/h$ ratio on the increase of the ultimate strength for various concrete strength.

For round-ended columns,

$$\frac{f_{cc}^{'}}{f_c^{'}} = -0.0579 \times (b/h)^3 + 0.5467 \times (b/h)^2 - 1.6513 \times (b/h) + 2.6962 \geqslant 1.13 \tag{43}$$

where, confinement factor ($\xi$) is calculated as $\xi = A_s\sigma_{0.2}/A_c\gamma_c f_c^{'}$, in which, the area of steel and concrete is characterized by $A_s$ and $A_c$, respectively calculated using Eqs. (1–2). Fig. 4 shows the accuracy of the proposed formulas for $f_{cc}^{'}/f_c^{'}$ against the test results.

The compressive strain of the confined concrete ($\varepsilon_{cc}^{'}$) is calculated as [88]:

$$\varepsilon_{cc}^{'} = \begin{cases} 3000 - 10.4(\sigma_{0.2})^{1.4}\left(\gamma_c f_c^{'}\right)^{-1.2}\left[0.73 - 3785.8\left(\frac{2(R_e+t_e)}{t_e}\right)^{-1.5}\right] \leqslant 0.01 \text{ for circular shape} \\ 2300 + 31.2\left(\gamma_c f_c^{'}\right)^{0.7} + \left[2.32\times10^4 - 3.88\times10^6\left(\gamma_c f_c^{'}\right)^{-1.8}\right]\left(\frac{t_e\sigma_{0.2}}{2(R_e+t_e)\gamma_c f_c^{'}}\right)^2 \text{ for other shapes} \end{cases} \tag{44}$$

The residual strength of concrete ($f_{cr}$) is calculated as $f_{cr} = \beta_c f_{cc}^{'}$, where $\beta_c (0 \leqslant \beta_c \leqslant 1)$ is the strength reduction factor. In determining, formulas for $\beta_c$, trial and error method was used to first determine the test value of $\beta_c$ to best fit the load-axial strain curves of tested columns collected for the verification purposes, listed in Tables 1 to 3. It should be noted that for rectangular and round-ended cross-sections of CFSST columns, local buckling of rectangular flat steel plates was considered, similar to the studies carried out by the authors previously [22,64] using the local buckling formulas proposed by Liang et al. [84] taking account for the residual stress of steel tube induced by welding. A regression analysis was then performed to express a formula for $\beta_c$ proposed in this study as

$$\beta_c = \begin{cases} 1.2420 - 0.0029\left(\frac{h}{t}\right) - 0.0044 f_c^{'} \text{ (circular shape)} \\ 0.459\xi + 0.046 \text{ (rectangular and square shapes)} \end{cases} \tag{45}$$

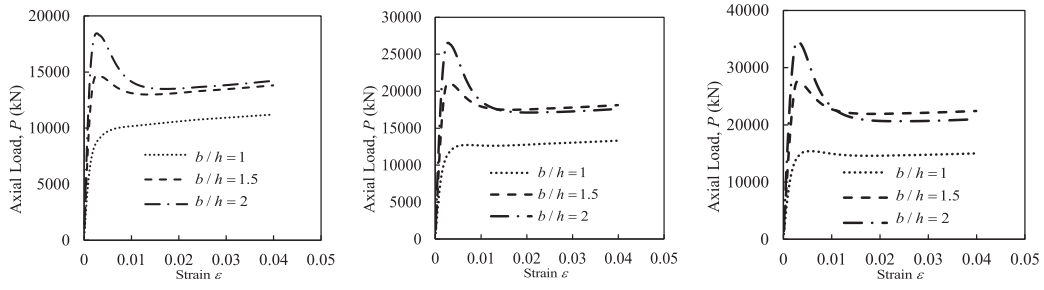


**Fig. 11.** Sensitivity of strength of concrete on the $P-\varepsilon$ curves for varying $b/h$ ratio.

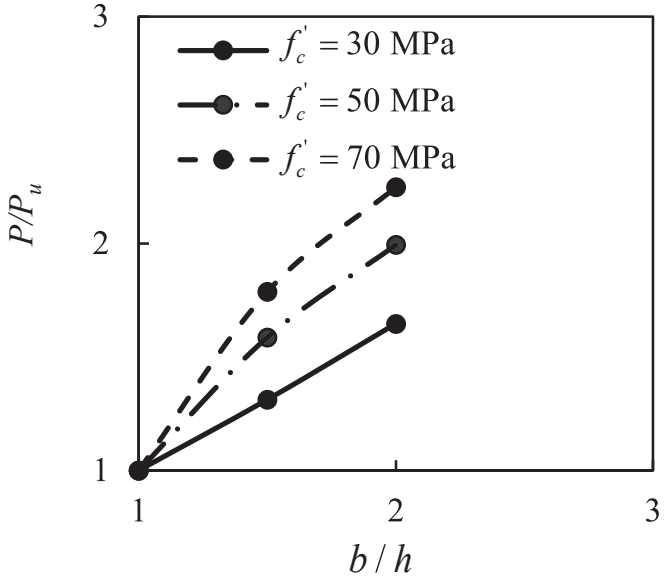


**Fig. 12.** Sensitivity of $b/h$ ratio on the increase of the ultimate strength for various concrete strength.

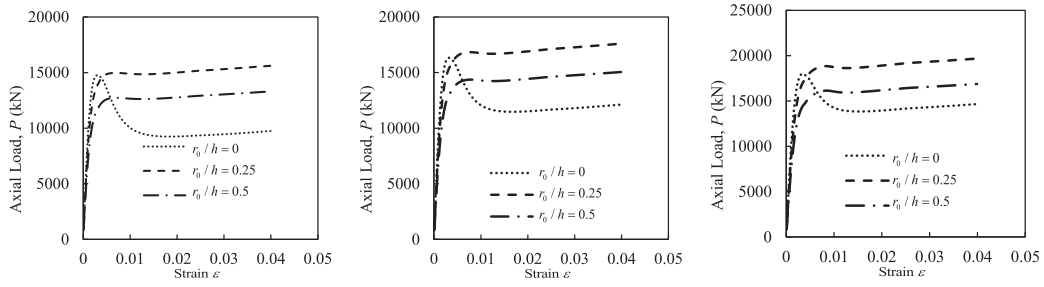


**Fig. 13.** Sensitivity of steel proof strength on the $P-\varepsilon$ curves for varying $r_0/h$ ratio.

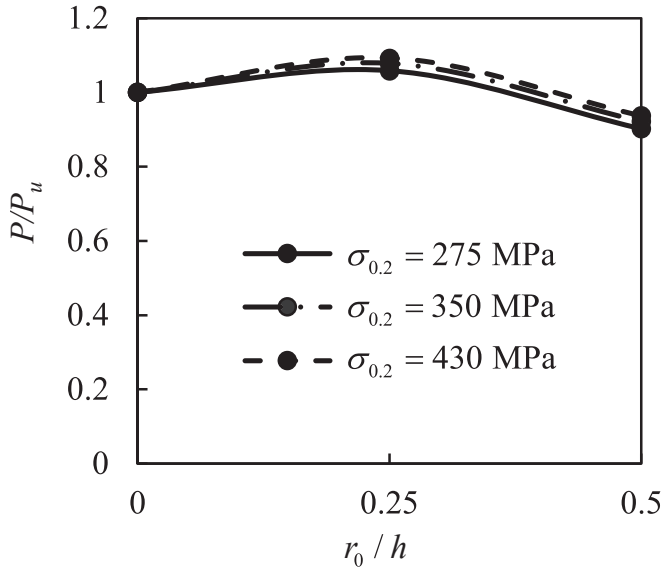


**Fig. 14.** Sensitivity of $r_0/h$ ratio on the increase of the ultimate strength for various steel proof strength.

For the round-ended columns,

$$\beta_c = \begin{cases} 1.436 - 0.512(b/h) + 0.015\xi \text{ for } 1.2 \leqslant b/h \leqslant 2 \\ 0.4 \text{ for} 2 < b/h \leqslant 4.2 \end{cases} \quad (46)$$

The inflection strain ($\varepsilon_{ci}$) is specified in this study as 0.007 for rectangular and round-ended shapes and 0.01 for circular columns.

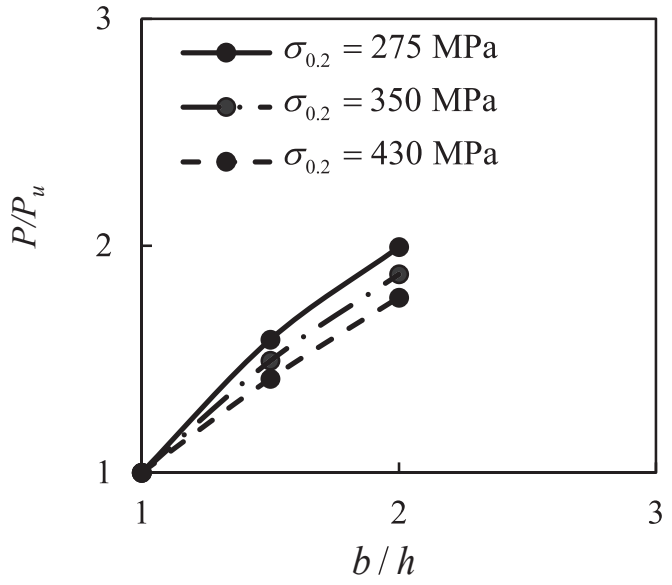


**Fig. 16.** Sensitivity of $b/h$ ratio on the increase of the ultimate strength for various steel proof strength.

## 4. Validation

The proposed unified model's accuracy is assessed by comparing its predicted ultimate load of CFSST columns with different cross-sections against test data in Tables 1-3. It is worth mentioning that the reported concrete cube strength was converted to cylindrical strength by multiplying by 0.85 [89]. It should be note that when stainless-steel's hardening exponent ($n$) was not reported, values suggested in AS/NZS 4673–2001 [90] were utilized in the computational analysis. The

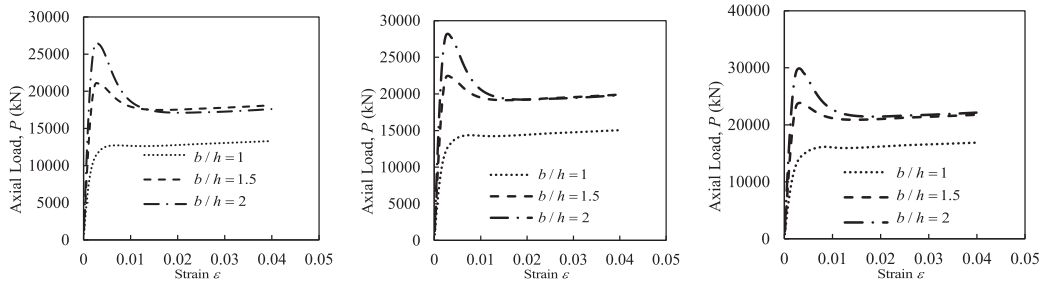


**Fig. 15.** Sensitivity of steel proof strength on the $P-\varepsilon$ curves for varying $b/h$ ratio.

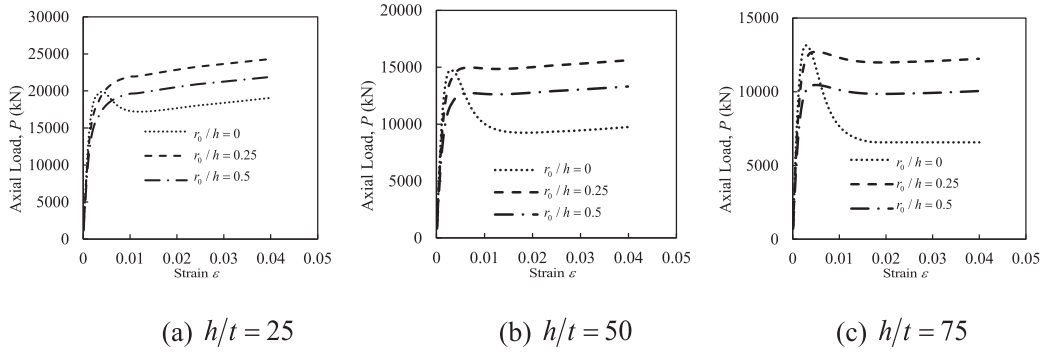


**Fig. 17.** Sensitivity of $h/t$ ratio on the $P-\varepsilon$ curves for varying $r_0/h$ ratio.

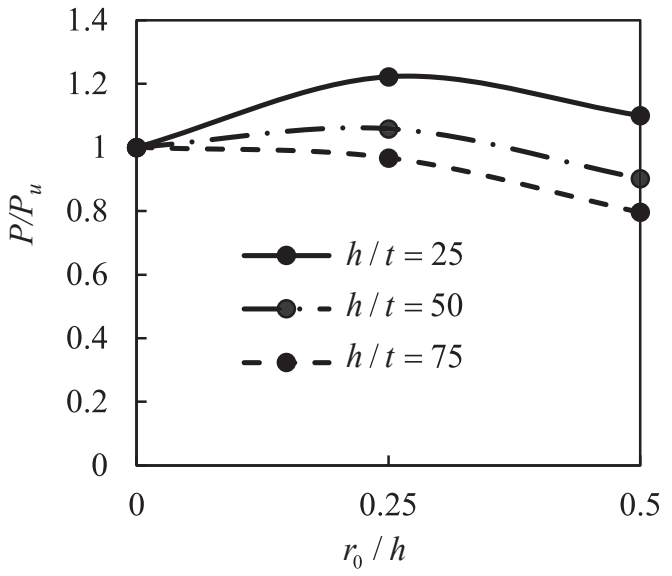


**Fig. 18.** Sensitivity of $r_0/h$ ratio on the increase of the ultimate strength for various $h/t$ ratio of the columns.

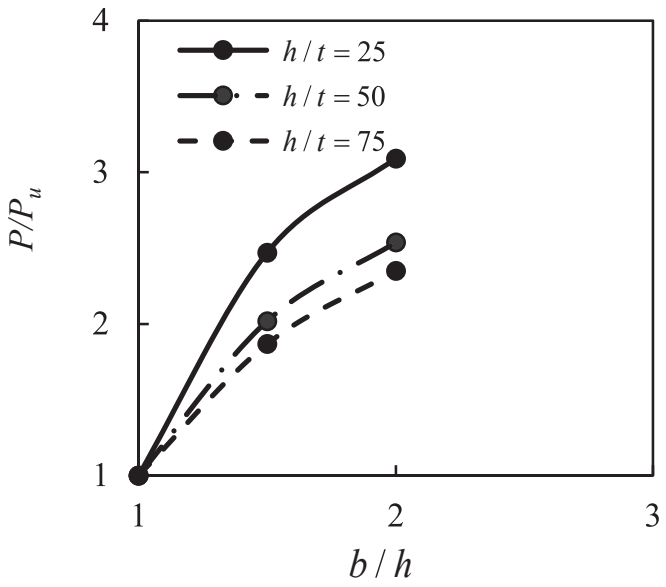


**Fig. 20.** Sensitivity of $b/h$ ratio on the increase of the ultimate strength for various $h/t$ ratio.

comparative study encompassed 196 tested columns with various cross-sections, including 80 circular, 87 rectangular/square, and 29 round-ended shapes. In the collected test data for circular columns, the range of parameters including: $50 \leqslant b \leqslant 325$ mm, $0.9 \leqslant t \leqslant 12$ mm, $19 \leqslant f_c' \leqslant 64$ MPa, $209 \leqslant \sigma_{0.2} \leqslant 542$ MPa, $0.2 \leqslant \xi \leqslant 2.87$ and $2.8 \leqslant L/b \leqslant 4.0$. For rectangular and square columns, the range of parameters including: $51 \leqslant b \leqslant 304$ mm, $40 \leqslant h \leqslant 304$ mm, $1 \leqslant t \leqslant 12.5$ mm, $19 \leqslant f_c' \leqslant 115$ MPa, $258 \leqslant \sigma_{0.2} \leqslant 634$ MPa, $0.4 \leqslant \xi \leqslant 4.8$ and $2.4 \leqslant L/b \leqslant 4.0$. It should be noted that in the absence of the test data on CFSST columns with round-ended shapes, experimental data of round-ended CFST columns with carbon steel was used for validation purposes where the range of parameters including: $120 \leqslant b \leqslant 806$ mm, $50 \leqslant h \leqslant 264$ mm, $2 \leqslant t \leqslant 6$ mm, $32 \leqslant f_c' \leqslant 49$ MPa, $300 \leqslant \sigma_{0.2} \leqslant 324$ MPa, $0.4 \leqslant \xi \leqslant 0.9$ and $2.0 \leqslant L/b \leqslant 3.2$. The stress–strain model of carbon steel used by Ahmed and Liang [22] was adopted in the computational modeling. As can be seen from the comparisons presented in Tables 1-3, the unified model developed can

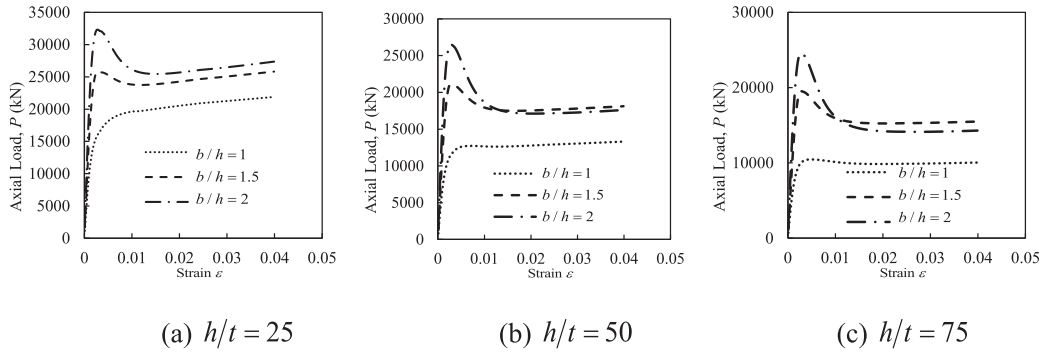


**Fig. 19.** Sensitivity of $h/t$ ratio on the $P-\varepsilon$ curves for varying $b/h$ ratio.

**Table 4**
Summary of the design specifications given by various design codes.

| Design Codes | Formulas to calculate the ultimate strength |
|---|---|
| AISC 360–16 [27] | $P_{u,AISC} = \begin{cases} P_o\left[0.658^{(P_o/P_e)}\right] \text{ for } P_e \geq 0.44P_o \\ 0.877P_e \text{ for } P_e < 0.44P_o \end{cases}$ |
| | $P_o = \sigma_{0.2}A_s + C_2A_cf_c'$ |
| | $P_e = \frac{\pi^2}{(KL)^2}(EI)_{eff}$ |
| | $(EI)_{eff} = E_{cs}I_{cs} + E_{ss}I_{ss} + C_4E_cI_c$ |
| | $C_4 = 0.6 + 2\left(\frac{A_s}{A_s + A_c}\right) \leqslant 0.9$ |
| | where $C_2 = \begin{cases} 0.85 \text{ for circular columns} \\ 0.95 \text{ for rectangular columns} \end{cases}$ |
| Eurocode 4 [26] | For circular columns: |
| | $P_{u,EC4} = \eta_a A_s\sigma_{0.2} + A_cf_c'(1 + \eta_c\frac{t}{D}\frac{\sigma_{0.2}}{f_c'})$ |
| | $\eta_a = 0.25(3 + 2\bar{\lambda})\eta_a \leqslant 1.0)$ |
| | $\eta_c = 4.9 - 18.5\bar{\lambda} + 17\bar{\lambda}^2\eta_c > 0)$ |
| | $\bar{\lambda} = \sqrt{\frac{N_{pl,Rk}}{N_{cr}}}$ |
| | For rectangular columns: |
| | $P_{u,EC4} = \sigma_{0.2}A_s + A_cf_c'$ |
| ACI 318–19 [28] | $P_{u,ACI} = A_s\sigma_{0.2} + 0.85A_cf_c'$ |
| DBJ 13–51-2010 [29] | $P_{u,DBJ} = f_{sc}(A_s + A_c)f_{sc} =$ $\begin{cases} f_{ck}(1.14 + 1.02\xi) \text{ circular columns} \\ f_{ck}(1.18 + 0.85\xi) \text{ rectangular columns} \end{cases} f_{ck} = 0.67f_{cu}$ |

accurately predict the ultimate strength of the CFSST columns. The mean value of $P_{u,num}/P_{u,exp}$ for different cross-sections scatter within ± 10%. Considering the significant strain hardening performance of CFSST columns particularly for the circular cross-section and as the comparisons of the ultimate strength was made at the maximum strain recorded during the test, the model overestimated the ultimate strength of some columns. The average value of $P_{u,num}/P_{u,exp}$ for circular, rectangular and round-ended columns was calculated as 1.00, 0.97 and 0.99, respectively. Fig. 5 shows the comparison of the predicted and test ultimate strength of all columns, and the mean $P_{u,num}/P_{u,exp}$ was calculated as 0.99 with standard deviation of 0.07.

To confirm the accuracy of the model, the estimated $P-\varepsilon$ curves for various cross-sections are compared with equivalent circular columns with test results, shown in Figs. 6-8. The comparisons reveal an excellent match between the numerical predictions and the tests, indicating that the material laws of concrete developed can accurately predict the post-peak behavior of confined concrete. Furthermore, the stainless steel model adopted can accurately predict the significant strain hardening performance of CFSST columns. In addition, the accuracy of the unified model developed is evaluated against the unified model developed by Lin et al. [72]. The comparison shows that there is a significant deviations between the test and the predicted ultimate strength of CFSST columns for the unified model developed by Lin et al. [72]. The mean $P_{u,Lin}/P_{u,exp}$ for all tested columns is calculated as 0.99 with a standard deviation of 0.14. Moreover, based on the comparison of the predicted $P-\varepsilon$ curves with the unified model developed by Lin et al. [72]

**Table 5**
Validation of the accuracy of the unified design model for estimating the ultimate strength of circular CFSST columns.

| Specimen | $P_{u,exp}$ (kN) | $P_{u,des}$ (kN) | $\frac{P_{u,des}}{P_{u,exp}}$ | $P_{u,EC4}$ (kN) | $P_{u,ACI}$(kN) | $P_{u,AISC}$(kN) | $P_{u,DBJ}$(kN) | $\frac{P_{u,EC4}}{P_{u,exp}}$ | $\frac{P_{u,ACI}}{P_{u,exp}}$ | $\frac{P_{u,AISC}}{P_{u,exp}}$ | $\frac{P_{u,DBJ}}{P_{u,exp}}$ |
|---|---|---|---|---|---|---|---|---|---|---|---|
| CHS104 × 2-C30 | 650 | 584 | 0.90 | 682 | 471 | 492 | 468 | 1.05 | 0.72 | 0.76 | 0.72 |
| CHS114 × 6-C60 | 1354 | 1149 | 0.85 | 1285 | 887 | 922 | 1004 | 0.95 | 0.65 | 0.68 | 0.74 |
| C30-50 × 1.6A | 167 | 154 | 0.92 | 177 | 119 | 124 | 122 | 1.06 | 0.71 | 0.74 | 0.73 |
| C30-50 × 1.6B | 162 | 154 | 0.95 | 177 | 119 | 124 | 122 | 1.09 | 0.74 | 0.76 | 0.75 |
| C30-100 × 1.6A | 477 | 436 | 0.91 | 501 | 355 | 375 | 357 | 1.05 | 0.74 | 0.79 | 0.75 |
| C30-100 × 1.6B | 477 | 436 | 0.91 | 501 | 355 | 375 | 357 | 1.05 | 0.74 | 0.79 | 0.75 |
| A1 | 4603 | 4686 | 1.02 | 5235 | 3651 | 3844 | 4052 | 1.14 | 0.79 | 0.84 | 0.88 |
| A2 | 4950 | 5211 | 1.05 | 5808 | 3984 | 4171 | 4513 | 1.17 | 0.80 | 0.84 | 0.91 |
| A3 | 5247 | 5907 | 1.13 | 6549 | 4433 | 4611 | 5124 | 1.25 | 0.84 | 0.88 | 0.98 |
| A6 | 5400 | 6104 | 1.13 | 6753 | 4619 | 4818 | 5357 | 1.25 | 0.86 | 0.89 | 0.99 |
| A7 | 4750 | 5057 | 1.06 | 5624 | 4001 | 4231 | 4465 | 1.18 | 0.84 | 0.89 | 0.94 |
| D2 | 11,032 | 10,528 | 0.95 | 11,196 | 7634 | 7830 | 8454 | 1.01 | 0.69 | 0.71 | 0.77 |
| D3 | 12,926 | 12,023 | 0.93 | 12,665 | 8606 | 8787 | 9726 | 0.98 | 0.67 | 0.68 | 0.75 |
| C-3-L-RS-1 | 1264 | 1391 | 1.10 | 1590 | 1129 | 1188 | 1168 | 1.26 | 0.89 | 0.94 | 0.92 |
| C-3-L-RS-2 | 1322 | 1391 | 1.05 | 1590 | 1129 | 1188 | 1168 | 1.20 | 0.85 | 0.90 | 0.88 |
| C-3-H-RS-1 | 1349 | 1495 | 1.11 | 1700 | 1227 | 1297 | 1280 | 1.26 | 0.91 | 0.96 | 0.95 |
| C-3-H-RS-2 | 1316 | 1495 | 1.14 | 1700 | 1227 | 1297 | 1280 | 1.29 | 0.93 | 0.99 | 0.97 |
| C-4-L-RS-1 | 1627 | 1696 | 1.04 | 1894 | 1315 | 1372 | 1368 | 1.16 | 0.81 | 0.84 | 0.84 |
| C-4-L-RS-2 | 1624 | 1696 | 1.04 | 1894 | 1315 | 1372 | 1368 | 1.17 | 0.81 | 0.84 | 0.84 |
| C-5-L-RS-1 | 1713 | 1880 | 1.10 | 2093 | 1438 | 1492 | 1509 | 1.22 | 0.84 | 0.87 | 0.88 |
| C-5-L-RS-2 | 1630 | 1880 | 1.15 | 2093 | 1438 | 1492 | 1509 | 1.28 | 0.88 | 0.92 | 0.93 |
| C-3-L-DS-1 | 1310 | 1391 | 1.06 | 1590 | 1129 | 1188 | 1168 | 1.21 | 0.86 | 0.91 | 0.89 |
| C-3-L-DS-2 | 1291 | 1391 | 1.08 | 1590 | 1129 | 1188 | 1168 | 1.23 | 0.87 | 0.92 | 0.90 |
| C-3-H-DS-1 | 1514 | 1495 | 0.99 | 1700 | 1227 | 1297 | 1280 | 1.12 | 0.81 | 0.86 | 0.85 |
| C-3-H-DS-2 | 1552 | 1495 | 0.96 | 1700 | 1227 | 1297 | 1280 | 1.10 | 0.79 | 0.84 | 0.82 |
| C-4-L-DS-1 | 1598 | 1696 | 1.06 | 1894 | 1315 | 1372 | 1368 | 1.19 | 0.82 | 0.86 | 0.86 |
| C-4-L-DS-2 | 1612 | 1696 | 1.05 | 1894 | 1315 | 1372 | 1368 | 1.17 | 0.82 | 0.85 | 0.85 |
| C-5-L-DS-1 | 1725 | 1880 | 1.09 | 2093 | 1438 | 1492 | 1509 | 1.21 | 0.83 | 0.87 | 0.87 |
| C-5-L-DS-2 | 1739 | 1880 | 1.08 | 2093 | 1438 | 1492 | 1509 | 1.20 | 0.83 | 0.86 | 0.87 |
| C-3-L-SS-1 | 1366 | 1391 | 1.02 | 1590 | 1129 | 1188 | 1168 | 1.16 | 0.83 | 0.87 | 0.85 |
| C-3-L-SS-2 | 1333 | 1391 | 1.04 | 1590 | 1129 | 1188 | 1168 | 1.19 | 0.85 | 0.89 | 0.88 |
| C-3-H-SS-1 | 1466 | 1495 | 1.02 | 1700 | 1227 | 1297 | 1280 | 1.16 | 0.84 | 0.88 | 0.87 |
| C-3-H-SS-2 | 1452 | 1495 | 1.03 | 1700 | 1227 | 1297 | 1280 | 1.17 | 0.85 | 0.89 | 0.88 |
| C-4-L-SS-1 | 1642 | 1696 | 1.03 | 1894 | 1315 | 1372 | 1368 | 1.15 | 0.80 | 0.84 | 0.83 |
| C-4-L-SS-2 | 1648 | 1696 | 1.03 | 1894 | 1315 | 1372 | 1368 | 1.15 | 0.80 | 0.83 | 0.83 |
| C-5-L-SS-1 | 1746 | 1880 | 1.08 | 2093 | 1438 | 1492 | 1509 | 1.20 | 0.82 | 0.85 | 0.86 |
| C-5-L-SS-2 | 1715 | 1880 | 1.10 | 2093 | 1438 | 1492 | 1509 | 1.22 | 0.84 | 0.87 | 0.88 |
| S50-C | 210 | 202 | 0.96 | 229 | 153 | 158 | 175 | 1.09 | 0.73 | 0.75 | 0.83 |
| S101-C | 555 | 516 | 0.93 | 571 | 417 | 439 | 438 | 1.03 | 0.75 | 0.79 | 0.79 |
| S114-C | 741 | 694 | 0.94 | 773 | 555 | 583 | 576 | 1.04 | 0.75 | 0.79 | 0.78 |

(continued on next page)

**Table 5** (*continued*)

| Specimen | $P_{u,exp}$ (kN) | $P_{u,des}$ (kN) | $\frac{P_{u,des}}{P_{u,exp}}$ | $P_{u,EC4}$ (kN) | $P_{u,ACI}$(kN) | $P_{u,AISC}$(kN) | $P_{u,DBJ}$(kN) | $\frac{P_{u,EC4}}{P_{u,exp}}$ | $\frac{P_{u,ACI}}{P_{u,exp}}$ | $\frac{P_{u,AISC}}{P_{u,exp}}$ | $\frac{P_{u,DBJ}}{P_{u,exp}}$ |
|---|---|---|---|---|---|---|---|---|---|---|---|
| S165-C | 1449 | 1355 | 0.94 | 1572 | 1096 | 1165 | 1155 | 1.08 | 0.76 | 0.80 | 0.80 |
| 50x1.6-F | 198 | 189 | 0.96 | 213 | 148 | 154 | 152 | 1.07 | 0.75 | 0.78 | 0.77 |
| 50x3-F | 226 | 212 | 0.94 | 239 | 162 | 168 | 187 | 1.06 | 0.72 | 0.74 | 0.83 |
| 76x1.6-F | 388 | 380 | 0.98 | 429 | 304 | 319 | 308 | 1.11 | 0.78 | 0.82 | 0.79 |
| 89x3-F | 548 | 528 | 0.96 | 599 | 417 | 437 | 446 | 1.09 | 0.76 | 0.80 | 0.81 |
| 101x1.6-F | 617 | 551 | 0.89 | 634 | 460 | 488 | 470 | 1.03 | 0.75 | 0.79 | 0.76 |
| 101x3-F | 610 | 558 | 0.92 | 638 | 456 | 484 | 485 | 1.05 | 0.75 | 0.79 | 0.79 |
| 114x3-F | 831 | 747 | 0.90 | 844 | 604 | 639 | 634 | 1.02 | 0.73 | 0.77 | 0.76 |
| 152x1.6-F | 1050 | 934 | 0.89 | 1137 | 864 | 930 | 903 | 1.08 | 0.82 | 0.89 | 0.86 |
| 203x2-F | 1787 | 1606 | 0.90 | 1945 | 1489 | 1606 | 1570 | 1.09 | 0.83 | 0.90 | 0.88 |
| C-S-N | 823 | 790 | 0.96 | 885 | 676 | 727 | 713 | 1.08 | 0.82 | 0.88 | 0.87 |
| C-S-C1 | 813 | 759 | 0.93 | 852 | 647 | 695 | 680 | 1.05 | 0.80 | 0.86 | 0.84 |
| C-S-C2 | 802 | 740 | 0.92 | 832 | 629 | 675 | 660 | 1.04 | 0.78 | 0.84 | 0.82 |
| C-S-C3 | 774 | 736 | 0.95 | 828 | 625 | 671 | 656 | 1.07 | 0.81 | 0.87 | 0.85 |
| C-S-F1 | 806 | 750 | 0.93 | 843 | 639 | 686 | 671 | 1.05 | 0.79 | 0.85 | 0.83 |
| C-S-F2 | 768 | 731 | 0.95 | 823 | 621 | 666 | 651 | 1.07 | 0.81 | 0.87 | 0.85 |
| C-S-F3 | 777 | 724 | 0.93 | 814 | 614 | 658 | 643 | 1.05 | 0.79 | 0.85 | 0.83 |
| C-100S | 552 | 517 | 0.94 | 583 | 446 | 482 | 474 | 1.06 | 0.81 | 0.87 | 0.86 |
| C-150S | 1138 | 1088 | 0.96 | 1219 | 947 | 1026 | 1014 | 1.07 | 0.83 | 0.90 | 0.89 |
| C-200S | 1868 | 1828 | 0.98 | 2016 | 1596 | 1736 | 1711 | 1.08 | 0.85 | 0.93 | 0.92 |
| C5 | 591 | 541 | 0.92 | 615 | 439 | 464 | 449 | 1.04 | 0.74 | 0.79 | 0.76 |
| D73-C50 | 375 | 391 | 1.04 | 443 | 312 | 327 | 340 | 1.18 | 0.83 | 0.87 | 0.91 |
| D73-C60 | 455 | 434 | 0.95 | 488 | 352 | 372 | 390 | 1.07 | 0.77 | 0.82 | 0.86 |
| D89-C60 | 685 | 701 | 1.02 | 783 | 564 | 594 | 610 | 1.14 | 0.82 | 0.87 | 0.89 |
| C-3–0.9–3.0 | 135 | 127 | 0.94 | 157 | 106 | 111 | 103 | 1.16 | 0.79 | 0.82 | 0.77 |
| C-3–1.0–3.0 | 152 | 143 | 0.94 | 173 | 116 | 121 | 113 | 1.14 | 0.76 | 0.80 | 0.74 |
| C-3–1.2–3.0 | 163 | 183 | 1.12 | 221 | 146 | 150 | 140 | 1.36 | 0.89 | 0.92 | 0.86 |
| C-4–0.9–3.0 | 155 | 135 | 0.87 | 165 | 114 | 120 | 112 | 1.07 | 0.74 | 0.77 | 0.72 |
| C-4–1.0–3.0 | 185 | 151 | 0.82 | 182 | 124 | 130 | 121 | 0.98 | 0.67 | 0.70 | 0.66 |
| C-3–0.9–3.5 | 128 | 127 | 0.99 | 153 | 106 | 111 | 103 | 1.19 | 0.83 | 0.87 | 0.81 |
| C-3–1.0–3.5 | 140 | 143 | 1.02 | 169 | 116 | 121 | 113 | 1.20 | 0.83 | 0.86 | 0.80 |
| C-3–1.2–3.5 | 160 | 183 | 1.14 | 214 | 146 | 150 | 140 | 1.34 | 0.91 | 0.94 | 0.87 |
| C-4–0.9–3.5 | 135 | 135 | 1.00 | 161 | 114 | 119 | 112 | 1.20 | 0.84 | 0.89 | 0.83 |
| C-4–1.0–3.5 | 165 | 151 | 0.92 | 177 | 124 | 129 | 121 | 1.07 | 0.75 | 0.78 | 0.73 |
| C-4–1.2–3.5 | 185 | 191 | 1.03 | 223 | 153 | 158 | 148 | 1.20 | 0.83 | 0.86 | 0.80 |
| C-3–1.0–4.0 | 158 | 143 | 0.91 | 164 | 116 | 120 | 113 | 1.04 | 0.73 | 0.76 | 0.71 |
| C-3–1.2–4.0 | 168 | 183 | 1.09 | 208 | 146 | 150 | 140 | 1.24 | 0.87 | 0.89 | 0.83 |
| C-4–0.9–4.0 | 135 | 135 | 1.00 | 158 | 114 | 119 | 112 | 1.17 | 0.84 | 0.88 | 0.83 |
| C-4–1.0–4.0 | 165 | 151 | 0.92 | 173 | 124 | 129 | 121 | 1.05 | 0.75 | 0.78 | 0.73 |
| C-4–1.2–4.0 | 200 | 191 | 0.95 | 217 | 153 | 158 | 148 | 1.08 | 0.77 | 0.79 | 0.74 |
| **Mean** | | | 0.99 | | | | | 1.13 | 0.80 | 0.84 | 0.83 |
| **SD** | | | 0.08 | | | | | 0.09 | 0.06 | 0.06 | 0.07 |
| **CoV** | | | 0.08 | | | | | 0.08 | 0.07 | 0.08 | 0.08 |

presented in Figs. 6-8, it is evident that the unified model developed in this study can provide more accurate results than that of Lin et al. [72].

## 5. Parametric study

The unified model is used to study the influences of concrete, steel yield stress and the depth-to-thisness ($h/t$) ratio for the various radius ratio ($r_0/h$) and aspect ratios ($b/h$) of CFSST columns under axial load. It should be noted that when $b/h = 1$ and $r_0/h = 0.5$, the cross-sectional shape of the column is circular. Similarly, for a column with $b/h > 1$ and $r_0/h = 0.5$ is considered round-ended, for a column with $b/h = 1$ and $r_0/h = 0$ is considered square and a column with $b/h > 1$ and $r_0/h = 0$ is considered rectangular. The geometry and material properties of the reference column are taken as: $b = h = 500$ mm, $t = 10$ mm, $r_0/h = 0.5$, $\sigma_{0.2} = 275$ MPa, $f_c^{'} = 50$ MPa.

### 5.1. Effects of concrete strength

The developed unified model was used to analyze the effect of concrete strength on the CFSST column. The concrete strength was varied between 30 MPa and 70 MPa. The results obtained from Figs. 9 and 10 show that the ultimate load increases as the $r_0/h$ ratio increases from 0 to 0.25, but then decreases as the ratio $r_0/h$ increases further. It should be noted that in Fig. 10, the benchmark ultimate strength of the columns for various concrete strengths is taken as the ultimate strength of the column with $r_0/h$ ratio equal 0. With the increase of the $r_0/h$ ratio, the cross-sectional area of the column decreases, which results in the reduction of the ultimate strength of the columns. However, the confinement to the core concrete increases with the increase of the $r_0/h$ ratio. The results show that for columns with a $r_0/h$ ratio less than or equal to 0.25, the higher confinement effects can compensate for the reduction of the load-carrying capacity due to the reduction of the cross-sectional area, especially for normal strength concrete. However, for an increase in the concrete strength, the confinement effects diminish, and the increase of the ultimate load becomes insignificant. Additionally, increasing the $r_0/h$ ratio of the columns increases the ductility of the columns, as shown in Figs. 11-12. The ultimate load of the columns increases with the increase in $b/h$ ratio regardless of the concrete strength. However, columns' ductility decreases. The benchmark ultimate strength of the columns for various concrete strengths is taken as the ultimate strength of the column with $b/h$ ratio equal to 1 in Fig. 12. The rate of increase in the ultimate load seems to be linear, as illustrated in Fig. 12.

### 5.2. Effects of steel proof strength

The study investigates the effects of steel proof strength by altering the proof stress withing the range of 275 to 430 MPa. The results shown in Figs. 13-14 indicate that increasing the $r_0/h$ ratio from 0 to 0.25

**Table 6**
Validation of the accuracy of the unified design model for estimating the ultimate strength of rectangular CFSST columns.

| Specimen | $P_{u,exp}$ (kN) | $P_{u,des}$ (kN) | $\frac{P_{u,des}}{P_{u,exp}}$ | $P_{u,EC4}$ (kN) | $P_{u,ACI}$(kN) | $P_{u,AISC}$(kN) | $P_{u,DBJ}$(kN) | $\frac{P_{u,EC4}}{P_{u,exp}}$ | $\frac{P_{u,ACI}}{P_{u,exp}}$ | $\frac{P_{u,AISC}}{P_{u,exp}}$ | $\frac{P_{u,DBJ}}{P_{u,exp}}$ |
|---|---|---|---|---|---|---|---|---|---|---|---|
| SHS1C40 | 2768 | 2866 | 1.04 | 2576 | 2441 | 2415 | 2394 | 0.93 | 0.88 | 0.87 | 0.87 |
| SHS1C60 | 2972 | 3074 | 1.03 | 2871 | 2692 | 2661 | 2717 | 0.97 | 0.91 | 0.90 | 0.91 |
| SHS1C80 | 3020 | 3398 | 1.13 | 3287 | 3046 | 3009 | 3172 | 1.09 | 1.01 | 1.00 | 1.05 |
| S30-50 × 2A | 268 | 226 | 0.84 | 204 | 192 | 191 | 182 | 0.76 | 0.72 | 0.71 | 0.68 |
| S30-50 × 2B | 274 | 226 | 0.83 | 204 | 192 | 191 | 182 | 0.74 | 0.70 | 0.70 | 0.66 |
| S20-100 × 3A | 705 | 671 | 0.95 | 588 | 559 | 555 | 503 | 0.83 | 0.79 | 0.79 | 0.71 |
| S20-100 × 3B | 716 | 671 | 0.94 | 588 | 559 | 555 | 503 | 0.82 | 0.78 | 0.77 | 0.70 |
| S30-100 × 3A | 765 | 761 | 0.99 | 707 | 660 | 655 | 628 | 0.92 | 0.86 | 0.86 | 0.82 |
| S30-100 × 3B | 742 | 761 | 1.03 | 707 | 660 | 655 | 628 | 0.95 | 0.89 | 0.88 | 0.85 |
| S20-100 × 5A | 1352 | 1354 | 1.00 | 1021 | 994 | 985 | 908 | 0.76 | 0.74 | 0.73 | 0.67 |
| S20-100 × 5B | 1348 | 1354 | 1.00 | 1021 | 994 | 985 | 908 | 0.76 | 0.74 | 0.73 | 0.67 |
| S30-100 × 5A | 1434 | 1362 | 0.95 | 1131 | 1088 | 1078 | 1035 | 0.79 | 0.76 | 0.75 | 0.72 |
| S30-100 × 5B | 1461 | 1362 | 0.93 | 1131 | 1088 | 1078 | 1035 | 0.77 | 0.74 | 0.74 | 0.71 |
| S20-150 × 3A | 1035 | 939 | 0.91 | 916 | 847 | 841 | 817 | 0.88 | 0.82 | 0.81 | 0.79 |
| S20-150 × 3B | 1062 | 939 | 0.88 | 916 | 847 | 841 | 817 | 0.86 | 0.80 | 0.79 | 0.77 |
| S30-150 × 3A | 1074 | 1177 | 1.10 | 1203 | 1091 | 1082 | 1105 | 1.12 | 1.02 | 1.01 | 1.03 |
| S30-150 × 3B | 1209 | 1177 | 0.97 | 1203 | 1091 | 1082 | 1105 | 0.99 | 0.90 | 0.90 | 0.91 |
| S20-150 × 5B | 1798 | 1569 | 0.87 | 1372 | 1308 | 1299 | 1226 | 0.76 | 0.73 | 0.72 | 0.68 |
| S30-150 × 5A | 1947 | 1746 | 0.90 | 1636 | 1533 | 1520 | 1507 | 0.84 | 0.79 | 0.78 | 0.77 |
| S30-150 × 5B | 1976 | 1746 | 0.88 | 1636 | 1533 | 1520 | 1507 | 0.83 | 0.78 | 0.77 | 0.76 |
| SHS 100 × 100 × 5 – C30 | 1410 | 1394 | 0.99 | 1117 | 1080 | 1070 | 1008 | 0.79 | 0.77 | 0.76 | 0.72 |
| SHS 100 × 100 × 5 – C60 | 1488 | 1462 | 0.98 | 1289 | 1224 | 1211 | 1206 | 0.87 | 0.82 | 0.81 | 0.81 |
| SHS 100 × 100 × 5 – C100 | 1559 | 1593 | 1.02 | 1461 | 1371 | 1355 | 1403 | 0.94 | 0.88 | 0.87 | 0.90 |
| 304-t8C50 | 6290 | 5631 | 0.90 | 5826 | 5344 | 5301 | 5620 | 0.93 | 0.85 | 0.84 | 0.89 |
| 304-t10C50 | 7113 | 6470 | 0.91 | 6496 | 6015 | 5969 | 6388 | 0.91 | 0.85 | 0.84 | 0.90 |
| 304-t12C50 | 7924 | 7609 | 0.96 | 7383 | 6901 | 6849 | 7382 | 0.93 | 0.87 | 0.86 | 0.93 |
| 304-t8C70 | 6743 | 6828 | 1.01 | 7392 | 6675 | 6614 | 7243 | 1.10 | 0.99 | 0.98 | 1.07 |
| 304-t10C70 | 7947 | 7637 | 0.96 | 8063 | 7346 | 7282 | 8058 | 1.01 | 0.92 | 0.92 | 1.01 |
| 304-t12C70 | 8575 | 8728 | 1.02 | 8949 | 8233 | 8163 | 9096 | 1.04 | 0.96 | 0.95 | 1.06 |
| 304-t8C80 | 7436 | 7367 | 0.99 | 8085 | 7264 | 7193 | 7961 | 1.09 | 0.98 | 0.97 | 1.07 |
| 304-t10C80 | 8430 | 8168 | 0.97 | 8756 | 7935 | 7863 | 8796 | 1.04 | 0.94 | 0.93 | 1.04 |
| 304-t12C80 | 9257 | 9246 | 1.00 | 9642 | 8822 | 8743 | 9855 | 1.04 | 0.95 | 0.94 | 1.06 |
| 2205-t8C50 | 8771 | 9718 | 1.11 | 8954 | 8473 | 8368 | 8379 | 1.02 | 0.97 | 0.95 | 0.96 |
| 2205-t10C50 | 10,111 | 11,061 | 1.09 | 9921 | 9439 | 9327 | 9471 | 0.98 | 0.93 | 0.92 | 0.94 |
| 2205-t12C50 | 12,472 | 13,490 | 1.08 | 11,565 | 11,087 | 10,957 | 11,349 | 0.93 | 0.89 | 0.88 | 0.91 |
| 2205-t8C70 | 9686 | 10,720 | 1.11 | 10,517 | 9802 | 9671 | 10,001 | 1.09 | 1.01 | 1.00 | 1.03 |
| 2205-t10C70 | 10,820 | 11,979 | 1.11 | 11,489 | 10,771 | 10,635 | 11,140 | 1.06 | 1.00 | 0.98 | 1.03 |
| 2205-t12C70 | 12,560 | 14,207 | 1.13 | 13,117 | 12,407 | 12,252 | 13,063 | 1.04 | 0.99 | 0.98 | 1.04 |
| 2205-t8C80 | 9962 | 11,207 | 1.13 | 11,209 | 10,390 | 10,247 | 10,719 | 1.13 | 1.04 | 1.03 | 1.08 |
| 2205-t10C80 | 11,728 | 12,445 | 1.06 | 12,182 | 11,361 | 11,213 | 11,879 | 1.04 | 0.97 | 0.96 | 1.01 |
| 2205-t12C80 | 13,272 | 14,619 | 1.10 | 13,804 | 12,991 | 12,825 | 13,822 | 1.04 | 0.98 | 0.97 | 1.04 |
| S200635 | 131 | 132 | 1.01 | 126 | 116 | 115 | 108 | 0.96 | 0.89 | 0.88 | 0.83 |
| S200640 | 126 | 132 | 1.05 | 126 | 116 | 115 | 108 | 1.00 | 0.92 | 0.92 | 0.86 |
| S200830 | 190 | 205 | 1.08 | 199 | 181 | 180 | 173 | 1.05 | 0.96 | 0.95 | 0.91 |
| S200835 | 182 | 205 | 1.12 | 199 | 181 | 180 | 173 | 1.09 | 1.00 | 0.99 | 0.95 |
| S2001030 | 258 | 288 | 1.12 | 288 | 260 | 258 | 253 | 1.12 | 1.01 | 1.00 | 0.98 |
| S300840 | 211 | 236 | 1.12 | 234 | 211 | 209 | 206 | 1.11 | 1.00 | 0.99 | 0.98 |
| S-3-L-RS-2 | 1534 | 1719 | 1.12 | 1697 | 1564 | 1548 | 1522 | 1.11 | 1.02 | 1.01 | 0.99 |
| S-4-L-RS-1 | 2040 | 1957 | 0.96 | 1877 | 1747 | 1731 | 1701 | 0.92 | 0.86 | 0.85 | 0.83 |
| S-4-L-RS-2 | 1931 | 1957 | 1.01 | 1877 | 1747 | 1731 | 1701 | 0.97 | 0.90 | 0.90 | 0.88 |
| S-5-L-RS-1 | 2125 | 2301 | 1.08 | 2133 | 2006 | 1987 | 1946 | 1.00 | 0.94 | 0.94 | 0.92 |
| S-5-L-RS-2 | 2012 | 2301 | 1.14 | 2133 | 2006 | 1987 | 1946 | 1.06 | 1.00 | 0.99 | 0.97 |
| S-3-L-DS-1 | 1543 | 1719 | 1.11 | 1697 | 1564 | 1548 | 1522 | 1.10 | 1.01 | 1.00 | 0.99 |
| S-3-L-DS-2 | 1590 | 1719 | 1.08 | 1697 | 1564 | 1548 | 1522 | 1.07 | 0.98 | 0.97 | 0.96 |
| S-3-H-DS-1 | 1769 | 1841 | 1.04 | 1847 | 1691 | 1673 | 1672 | 1.04 | 0.96 | 0.95 | 0.95 |
| S-3-H-DS-2 | 1914 | 1841 | 0.96 | 1847 | 1691 | 1673 | 1672 | 0.96 | 0.88 | 0.87 | 0.87 |
| S-4-L-DS-1 | 1955 | 1957 | 1.00 | 1877 | 1747 | 1731 | 1701 | 0.96 | 0.89 | 0.89 | 0.87 |
| S-4-L-DS-2 | 1897 | 1957 | 1.03 | 1877 | 1747 | 1731 | 1701 | 0.99 | 0.92 | 0.91 | 0.90 |
| S-5-L-DS-1 | 2152 | 2301 | 1.07 | 2133 | 2006 | 1987 | 1946 | 0.99 | 0.93 | 0.92 | 0.90 |
| S-5-L-DS-2 | 2141 | 2301 | 1.07 | 2133 | 2006 | 1987 | 1946 | 1.00 | 0.94 | 0.93 | 0.91 |
| S-3-L-SS-1 | 1724 | 1719 | 1.00 | 1697 | 1564 | 1548 | 1522 | 0.98 | 0.91 | 0.90 | 0.88 |
| S-3-L-SS-2 | 1780 | 1719 | 0.97 | 1697 | 1564 | 1548 | 1522 | 0.95 | 0.88 | 0.87 | 0.85 |
| S-3-H-SS-1 | 1690 | 1841 | 1.09 | 1847 | 1691 | 1673 | 1672 | 1.09 | 1.00 | 0.99 | 0.99 |
| S-3-H-SS-2 | 1765 | 1841 | 1.04 | 1847 | 1691 | 1673 | 1672 | 1.05 | 0.96 | 0.95 | 0.95 |
| S-4-L-SS-1 | 2007 | 1957 | 0.97 | 1877 | 1747 | 1731 | 1701 | 0.94 | 0.87 | 0.86 | 0.85 |
| S-4-L-SS-2 | 1947 | 1957 | 1.00 | 1877 | 1747 | 1731 | 1701 | 0.96 | 0.90 | 0.89 | 0.87 |
| S-5-L-SS-1 | 2215 | 2301 | 1.04 | 2133 | 2006 | 1987 | 1946 | 0.96 | 0.91 | 0.90 | 0.88 |
| S-5-L-SS-2 | 2197 | 2301 | 1.05 | 2133 | 2006 | 1987 | 1946 | 0.97 | 0.91 | 0.90 | 0.89 |
| A100 | 698 | 662 | 0.95 | 630 | 583 | 579 | 577 | 0.90 | 0.83 | 0.83 | 0.83 |
| A250 | 2709 | 2686 | 0.99 | 2981 | 2655 | 2632 | 2782 | 1.10 | 0.98 | 0.97 | 1.03 |
| D100 | 1039 | 1047 | 1.01 | 929 | 881 | 872 | 809 | 0.89 | 0.85 | 0.84 | 0.78 |
| D250 | 3186 | 3589 | 1.13 | 3742 | 3414 | 3376 | 3403 | 1.17 | 1.07 | 1.06 | 1.07 |
| 60 × 40 × 4C40 | 478 | 539 | 1.13 | 409 | 398 | 395 | 414 | 0.86 | 0.83 | 0.83 | 0.87 |

(*continued on next page*)

**Table 6** (*continued*)

| Specimen | $P_{u,exp}$ (kN) | $P_{u,des}$ (kN) | $\frac{P_{u,des}}{P_{u,exp}}$ | $P_{u,EC4}$ (kN) | $P_{u,ACI}$(kN) | $P_{u,AISC}$(kN) | $P_{u,DBJ}$(kN) | $\frac{P_{u,EC4}}{P_{u,exp}}$ | $\frac{P_{u,ACI}}{P_{u,exp}}$ | $\frac{P_{u,AISC}}{P_{u,exp}}$ | $\frac{P_{u,DBJ}}{P_{u,exp}}$ |
|---|---|---|---|---|---|---|---|---|---|---|---|
| 60 × 40 × 4C40R | 481 | 539 | 1.12 | 408 | 397 | 394 | 413 | 0.85 | 0.83 | 0.82 | 0.86 |
| 60 × 40 × 4C80 | 531 | 555 | 1.05 | 474 | 453 | 449 | 499 | 0.89 | 0.85 | 0.85 | 0.94 |
| 60 × 40 × 4C120 | 585 | 593 | 1.01 | 530 | 501 | 496 | 574 | 0.91 | 0.86 | 0.85 | 0.98 |
| 60 × 60 × 3C40 | 484 | 482 | 1.00 | 416 | 397 | 393 | 379 | 0.86 | 0.82 | 0.81 | 0.78 |
| 60 × 60 × 3C80 | 594 | 569 | 0.96 | 529 | 493 | 487 | 507 | 0.89 | 0.83 | 0.82 | 0.85 |
| 80 × 60 × 4C40 | 712 | 721 | 1.01 | 605 | 581 | 576 | 563 | 0.85 | 0.82 | 0.81 | 0.79 |
| 80 × 60 × 4C80 | 878 | 824 | 0.94 | 753 | 706 | 700 | 735 | 0.86 | 0.80 | 0.80 | 0.84 |
| 80 × 60 × 4C120 | 999 | 932 | 0.93 | 881 | 815 | 807 | 885 | 0.88 | 0.82 | 0.81 | 0.89 |
| 80 × 60 × 4C120R | 976 | 932 | 0.96 | 881 | 815 | 807 | 885 | 0.90 | 0.84 | 0.83 | 0.91 |
| 100 × 40 × 2C40 | 398 | 401 | 1.01 | 366 | 344 | 342 | 326 | 0.92 | 0.86 | 0.86 | 0.82 |
| 100 × 40 × 2C120 | 674 | 624 | 0.93 | 617 | 557 | 554 | 594 | 0.92 | 0.83 | 0.82 | 0.88 |
| 120 × 80 × 3C40 | 870 | 827 | 0.95 | 776 | 722 | 717 | 696 | 0.89 | 0.83 | 0.82 | 0.80 |
| 120 × 80 × 3C80 | 1255 | 1115 | 0.89 | 1102 | 999 | 991 | 1039 | 0.88 | 0.80 | 0.79 | 0.83 |
| 120 × 80 × 3C120 | 1610 | 1375 | 0.85 | 1389 | 1243 | 1231 | 1339 | 0.86 | 0.77 | 0.76 | 0.83 |
| **Mean** | | | 1.01 | | | | | 0.96 | 0.89 | 0.88 | 0.89 |
| **SD** | | | 0.08 | | | | | 0.10 | 0.09 | 0.09 | 0.11 |
| **CoV** | | | 0.08 | | | | | 0.11 | 0.10 | 0.10 | 0.12 |

**Table 7**
Validation of the accuracy of the unified design model for estimating the ultimate strength of round-ended CFST columns.

| Specimen | $P_{u,exp}$ (kN) | $P_{u,des}$ (kN) | $\frac{P_{u,des}}{P_{u,exp}}$ | $P_{u,EC4}$ (kN) | $P_{u,ACI}$(kN) | $P_{u,AISC}$(kN) | $P_{u,DBJ}$(kN) | $\frac{P_{u,EC4}}{P_{u,exp}}$ | $\frac{P_{u,ACI}}{P_{u,exp}}$ | $\frac{P_{u,AISC}}{P_{u,exp}}$ | $\frac{P_{u,DBJ}}{P_{u,exp}}$ |
|---|---|---|---|---|---|---|---|---|---|---|---|
| WST1-A | 3429 | 3529 | 1.03 | 3768 | 2780 | 2923 | 2935 | 1.10 | 0.81 | 0.85 | 0.86 |
| WST1-B | 3328 | 3511 | 1.06 | 3764 | 2788 | 2926 | 2941 | 1.13 | 0.84 | 0.88 | 0.88 |
| WST2-A | 4162 | 3944 | 0.95 | 4469 | 3193 | 3335 | 3423 | 1.07 | 0.77 | 0.80 | 0.82 |
| WST2-B | 4168 | 3888 | 0.93 | 4407 | 3165 | 3301 | 3388 | 1.06 | 0.76 | 0.79 | 0.81 |
| WST3-A | 3929 | 3952 | 1.01 | 4346 | 3285 | 3429 | 3465 | 1.11 | 0.84 | 0.87 | 0.88 |
| WST3-B | 4158 | 3925 | 0.94 | 4334 | 3282 | 3421 | 3460 | 1.04 | 0.79 | 0.82 | 0.83 |
| WST4-A | 4492 | 4356 | 0.97 | 5052 | 3734 | 3867 | 3981 | 1.12 | 0.83 | 0.86 | 0.89 |
| WST4-B | 5530 | 4985 | 0.90 | 5583 | 4202 | 4368 | 4527 | 1.01 | 0.76 | 0.79 | 0.82 |
| WST5-A | 5620 | 5129 | 0.91 | 5586 | 4386 | 4563 | 4671 | 0.99 | 0.78 | 0.81 | 0.83 |
| WST5-B | 5500 | 5230 | 0.95 | 5689 | 4459 | 4643 | 4751 | 1.03 | 0.81 | 0.84 | 0.86 |
| WST6-A | 3240 | 3386 | 1.05 | 3915 | 3113 | 3183 | 3255 | 1.21 | 0.96 | 0.98 | 1.00 |
| WST7-A | 4826 | 4872 | 1.01 | 5282 | 4501 | 4495 | 4696 | 1.09 | 0.93 | 0.93 | 0.97 |
| WST7-B | 4944 | 4999 | 1.01 | 5444 | 4616 | 4621 | 4819 | 1.10 | 0.93 | 0.93 | 0.97 |
| WST8-A | 6521 | 6552 | 1.00 | 6910 | 6041 | 5922 | 6296 | 1.06 | 0.93 | 0.91 | 0.97 |
| WST8-B | 6493 | 6550 | 1.01 | 6908 | 6035 | 5918 | 6291 | 1.06 | 0.93 | 0.91 | 0.97 |
| WST9-A | 4203 | 4411 | 1.05 | 4950 | 4012 | 4113 | 4279 | 1.18 | 0.95 | 0.98 | 1.02 |
| WST9-B | 4180 | 4398 | 1.05 | 4931 | 3998 | 4100 | 4264 | 1.18 | 0.96 | 0.98 | 1.02 |
| WST10-A | 7201 | 6654 | 0.92 | 7141 | 6083 | 6087 | 6484 | 0.99 | 0.84 | 0.85 | 0.90 |
| WST10-B | 6905 | 6418 | 0.93 | 6871 | 5871 | 5861 | 6256 | 1.00 | 0.85 | 0.85 | 0.91 |
| WST11-A | 9065 | 8569 | 0.95 | 8974 | 7822 | 7629 | 8329 | 0.99 | 0.86 | 0.84 | 0.92 |
| WST11-B | 8799 | 8766 | 1.00 | 9193 | 8005 | 7824 | 8524 | 1.04 | 0.91 | 0.89 | 0.97 |
| RCFST-1 | 925 | 1036 | 1.12 | 1127 | 854 | 877 | 865 | 1.22 | 0.92 | 0.95 | 0.93 |
| RCFST-2 | 1215 | 1300 | 1.07 | 1417 | 1158 | 1170 | 1173 | 1.17 | 0.95 | 0.96 | 0.97 |
| RCFST-4 | 1658 | 1700 | 1.03 | 1843 | 1426 | 1469 | 1467 | 1.11 | 0.86 | 0.89 | 0.88 |
| RCFST-5 | 2091 | 2128 | 1.02 | 2333 | 1919 | 1944 | 1980 | 1.12 | 0.92 | 0.93 | 0.95 |
| RND_30_00 | 385 | 404 | 1.05 | 418 | 348 | 349 | 348 | 1.08 | 0.90 | 0.91 | 0.90 |
| **Mean** | | | 1.00 | | | | | 1.09 | 0.87 | 0.89 | 0.91 |
| **SD** | | | 0.06 | | | | | 0.07 | 0.07 | 0.06 | 0.06 |
| **CoV** | | | 0.06 | | | | | 0.06 | 0.08 | 0.07 | 0.07 |

increases the ultimate load, but beyond this range, the ultimate load decreases as the $r_0/h$ ratio increases. Moreover, the increase in the proof stress leads to a more significant rate of increase in the ultimate load. Regardless of the proof strength of the columns, the ductility of the column increases with an increase in the $r_0/h$ ratio, owing to the increase in the confinement effects. However, the ductility of the columns decreases as the $b/h$ ratio increases, as illustrated in Fig. 15. Fig. 16 reveals that the increase in the ultimate strength due to the increase in the $b/h$ ratio is linear for different proof strengths of the steel tube.

### 5.3. Effects of $h/t$ ratio of the columns

The effects of different $h/t$ ratios are explored by altering the thickness of the steel tube to vary $h/t$ ratio from 25 to 75. The results depicted in Figs. 17-18 show that, for a given $r_0/h$ ratio, increasing $h/t$ ratio decreases the ultimate strength of the columns. This is because the $h/t$ ratio is directly related to the confinement provided to the concrete core. The confinement effect occurs due to the confinement pressure exerted by the steel tube on the concrete core, which improves the strength and ductility of the column. A thinner steel tube which leads to higher $h/t$ ratio provides less confinement to the concrete, leading to reduced strength and ductility. Therefore, an increase in the $h/t$ ratio reduces the confinement effects, ultimately leading to a decrease in the ultimate axial strength. Although the ultimate strength of the column increases with an increase in $b/h$ ratio regardless of the $h/t$ ratio, the rate of increase declines as the $h/t$ ratio goes up, as shown in Figs. 19-20.

## 6. The ultimate strength of CFSST columns

### 6.1. Design codes

This section assesses the precision of the design specifications

outlined in four different codes, namely Eurocode 4 [26], ACI 318–11 [28], AISC 360–16 [27] and DBJ 13–51-2010 [29], for conventional CFST columns. The evaluation focuses on the ability of these codes to estimate the ultimate strength of CFSST columns with different cross-sectional shapes. The formulas specified by each code are summarized in Table 4. To evaluate their accuracy, the design predictions are compared with the test results presented in Tables 5-7. It should be noted that in the comparisons, the ultimate strength of the columns is taken as the axial load at 1% strain if the tested column had no obvious strain-softening branch [25,64,94,95]. Otherwise, the ultimate strength is taken as the maximum load for columns with an apparent strain-softening branch. The analysis reveals significant discrepancies between the actual and design predictions. Eurocode 4 [26] is observed to overestimate the ultimate strength of columns with circular and round-ended shapes while underestimating the ultimate strength of rectangular CFSST columns. Similarly, the other design codes substantially underestimate the ultimate strength of stub columns across all cross-sectional shapes.

### 6.2. Unified design model

Based on the unified numerical model, a unified design model to predict the maximum compressive load for various shapes of CFSST columns replaced by equivalent circular column theory is proposed herein as

$$P_{u,des} = A_s\sigma_{0.2} + A_c f_{cc}^{'} \tag{47}$$

The area of steel and concrete of the equivalent circular column is calculated using Eq. (1) and (2), respectively. The compressive strength of concrete ($f_{cc}^{'}$) for various cross-sections should be calculated using the formulas given in Eqs. (42)-(43). An excellent match between the test and the design prediction can be observed based on the comparison. The mean value of $P_{u,des}/P_{u,\exp}$ for circular, rectangular and round-ended columns are calculated as 0.99, 1.01 and 1.00, respectively. The proposed unified model can provide a more accurate design estimation of CFSST columns with various cross-sectional shapes.

## 7. Conclusions

A unified numerical model has been created in this paper to examine the performance of axially loaded CFSST stub columns, using various cross-sectional shapes. This model converts the different cross-sections of CFSST columns into equal circular columns, and incorporates a newly proposed formula for concrete compressive strength and a strength reduction factor to account for the residual strength of confined concrete. The accuracy of this unified model has been verified using a large data set collected from literature. An extensive parametric study is performed to study the effects of various column parameters on CFSST columns with various $r_0/h$ and $b/h$ ratios. The accuracy of the various design codes in predicting the ultimate strength of CFSST columns is studied and the accuracy of the proposed unified design model is examined. The following conclusions can be drawn from this study:

1. The unified model developed can predict the behavior of CFSST columns with different cross-sections accurately. The average value of $P_{u,num}/P_{u,\exp}$ for circular, rectangular and round-ended columns is calculated as 1.00, 0.97 and 0.99, respectively. For all columns, the mean $P_{u,num}/P_{u,\exp}$ is estimated as 0.99.
2. The developed model is validated for circular columns with $50\leqslant b\leqslant 325$ mm,$0.9\leqslant t\leqslant 12$ mm, $19\leqslant f_c^{'}\leqslant 64$ MPa, $209\leqslant\sigma_{0.2}\leqslant 542$ MPa, $0.2\leqslant\xi\leqslant 2.87$ and $2.8\leqslant L/b\leqslant 4.0$; for rectangular and square columns, the range of parameters including: $51\leqslant b\leqslant 304$ mm, $40\leqslant h\leqslant 304$ mm,$1\leqslant t\leqslant 12.5$ mm, $19\leqslant f_c^{'}\leqslant 115$ MPa, $258\leqslant\sigma_{0.2}\leqslant 634$ MPa, $0.4\leqslant\xi\leqslant 4.8$ and $2.4\leqslant L/b\leqslant 4.0$. Due to the absence of the test data on round-ended CFSST columns, the model is validated against the round-ended conventional CFST columns with $120\leqslant b\leqslant 806$ mm, $50\leqslant h\leqslant 264$ mm, $2\leqslant t\leqslant 6$ mm, $32\leqslant f_c^{'}\leqslant 49$ MPa, $300\leqslant\sigma_{0.2}\leqslant 324$ MPa, $0.4\leqslant\xi\leqslant 0.9$ and $2.0\leqslant L/b\leqslant 3.2$.
3. From the parametric study, it was found that the behavior of CFSST columns is influenced by $r_0/h$ and $b/h$ ratios of the columns. For a given $r_0/h$ ratio, increasing $h/t$ ratio decreases the ultimate strength of the columns. The ultimate load of the columns increases with the increase in $b/h$ ratio regardless of the concrete strength. In addition, regardless of the steel proof stress, increasing $b/h$ ratio increases the ultimate strength of the columns.
4. The proposed unified design model for determining the ultimate strength of CFSST columns with various cross-sections is more accurate than existing design codes.

## Declaration of Competing Interest

The authors declare that they have no known competing financial interests or personal relationships that could have appeared to influence the work reported in this paper.

## References


[1] Knowles RB, Park R. Strength of concrete filled steel columns. J Struct Div ASCE 1969;95(12):2565–87.
[2] Schneider SP. Axially loaded concrete-filled steel tubes. J Struct Eng 1998;124(10):1125–38.
[3] Hu HT, Huang CS, Wu MH, Wu YM. Nonlinear analysis of axially loaded concrete-filled tube columns with confinement effect. J Struct Eng 2003;129(10):1322–9.
[4] Giakoumelis G, Lam D. Axial capacity of circular concrete-filled tube columns. J Constr Steel Res 2004;60(7):1049–68.
[5] Dundu M. Compressive strength of circular concrete filled steel tube columns. Thin-Walled Struct 2012;56:62–70.
[6] Yang YF, Han LH. Concrete filled steel tube (CFST) columns subjected to concentrically partial compression. Thin-Walled Struct 2012;50(1):147–56.
[7] Portolés J, Serra E, Romero ML. Influence of ultra-high strength infill in slender concrete-filled steel tubular columns. J Constr Steel Res 2013;86:107–14.
[8] Ellobody E, Young B, Lam D. Behaviour of normal and high strength concrete-filled compact steel tube circular stub columns. J Constr Steel Res 2006;62(7):706–15.
[9] Liang QQ, Fragomeni S. Nonlinear analysis of circular concrete-filled steel tubular short columns under eccentric loading. J Constr Steel Res 2010;66(2):159–69.
[10] Shen M, Huang W, Liu J, Zhou Z. Axial compressive behavior of rubberized concrete-filled steel tube short columns. Case Stud Constr Mater 2022;16:e00851.
[11] Sakino K, Nakahara H, Morino S, Nishiyama I. Behavior of centrally loaded concrete-filled steel-tube short columns. J Struct Eng 2004;130(2):180–8.
[12] Wang Z, Chen J, Xie E, Lin S. Behavior of concrete-filled round-ended steel tubular stub columns under axial compression. Journal of Building Structures 2014;35(7):123–30. Chinese.
[13] Ding F-X, Li Z, Cheng S, Yu Z-W. Composite action of octagonal concrete-filled steel tubular stub columns under axial loading. Thin-Walled Struct 2016;107:453–61.
[14] Ding F-X, Li Z, Cheng S, Yu Z-W. Composite action of hexagonal concrete-filled steel tubular stub columns under axial loading. Thin-Walled Struct 2016;107:502–13.
[15] Xu W, Han L-H, Li W. Performance of hexagonal CFST members under axial compression and bending. J Constr Steel Res 2016;123:162–75.
[16] Hassanein MF, Patel VI, Bock M. Behaviour and design of hexagonal concrete-filled steel tubular short columns under axial compression. Eng Struct 2017;153:732–48.
[17] Hassanein MF, Patel VI, Elchalakani M, Thai H-T. Finite element analysis of large diameter high strength octagonal CFST short columns. Thin-Walled Struct 2018;123:467–82.
[18] Hassanein MF, Patel VI. Round-ended rectangular concrete-filled steel tubular short columns: FE investigation under axial compression. J Constr Steel Res 2018;140:222–36.
[19] Hassanein MF, Patel VI, El Hadidy AM, Al Abadi H, Elchalakani M. Structural behaviour and design of elliptical high-strength concrete-filled steel tubular short compression members. Eng Struct 2018;173:495–511.
[20] Ahmed M, Liang QQ. Numerical modeling of octagonal concrete-filled steel tubular short columns accounting for confinement effects. Eng Struct 2021;226:111405.
[21] Patel VI. Analysis of uniaxially loaded short round-ended concrete-filled steel tubular beam-columns. Eng Struct 2020;205:110098.
[22] Ahmed M, Liang QQ. Numerical analysis of thin-walled round-ended concrete-filled steel tubular short columns including local buckling effects. Structures 2020;28:181–96.
[23] Ahmed M, Liang QQ. Computational simulation of elliptical concrete-filled steel tubular short columns including new confinement model. J Constr Steel Res 2020;174:106294.
[24] Ahmed M, Liang QQ. Numerical analysis of concentrically loaded hexagonal concrete-filled steel tubular short columns incorporating concrete confinement. 13694332211004111 Adv Struct Eng 2021.

[25] Ahmed M, Ci J, Yan X-F, Chen S. Nonlinear analysis of elliptical concrete-filled stainless steel tubular short columns under axial compression. Structures 2021;32:1374–85.
[26] Eurocode 4: Design of Composite Steel and Concrete Structures-Part 1-1: General Rules and Rules for Buildings. European Committee for Standardization (CEN) Brussels, Belgium. 2004.
[27] AISC 360-16. Specification for Structural Steel Buildings. American Institute of Steel Construction. Chicago (IL), USA. 2016.
[28] ACI 318-19. Building Code Requirements for Structural Concrete and Commentary. Farmington Hills, Michigan, USA. 2019.
[29] DBJ 13-51-2010. Technical specifications for concrete-filled steel tubular structures. The Housing and Urban–Rural Development, Department of Fujian Province, Fuzhou, China. 2010.
[30] Young B, Ellobody E. Experimental investigation of concrete-filled cold-formed high strength stainless steel tube columns. J Constr Steel Res 2006;62(5):484–92.
[31] Lam D, Gardner L. Structural design of stainless steel concrete filled columns. J Constr Steel Res 2008;64(11):1275–82.
[32] Uy B, Tao Z, Han LH. Behaviour of short and slender concrete-filled stainless steel tubular columns. J Constr Steel Res 2011;67(3):360–78.
[33] Bambach M. Design of hollow and concrete filled steel and stainless steel tubular columns for transverse impact loads. Thin-Walled Struct 2011;49(10):1251–60.
[34] Ellobody E, Ghazy MF. Experimental investigation of eccentrically loaded fibre reinforced concrete-filled stainless steel tubular columns. J Constr Steel Res 2012;76:167–76.
[35] Yang Y-F, Ma G-L. Experimental behaviour of recycled aggregate concrete filled stainless steel tube stub columns and beams. Thin-Walled Struct 2013;66:62–75.
[36] Chen Y, Li F, Wang J. Experimental study on axial compressive behavior of concrete-filled thermoforming stainless steel tubular stub columns. Journal of Building Structures 2013;34(2):106–12.
[37] Chen Y, Huang Y. Experimental research on static behavior of welded concrete-filled stainless steel square stub columns under axial compression. Journal of Building Structures 2013;34(2):113–8.
[38] Yousuf M, Uy B, Tao Z, Remennikov A, Liew JR. Transverse impact resistance of hollow and concrete filled stainless steel columns. J Constr Steel Res 2013;82:177–89.
[39] Han L-H, Chen F, Liao F-Y, Tao Z, Uy B. Fire performance of concrete filled stainless steel tubular columns. Eng Struct 2013;56:165–81.
[40] Tam VW, Wang Z-B, Tao Z. Behaviour of recycled aggregate concrete filled stainless steel stub columns. Mater Struct 2014;47(1):293–310.
[41] Li Y, Zhao X, Singh RR, Al-Saadi S. Tests on seawater and sea sand concrete-filled CFRP, BFRP and stainless steel tubular stub columns. Thin-Walled Struct 2016;108:163–84.
[42] Li Y, Zhao X, Raman RS, Yu X. Axial compression tests on seawater and sea sand concrete-filled double-skin stainless steel circular tubes. Eng Struct 2018;176:426–38.
[43] Peng D, Lu Y, Xuan W, Yu-hang Z. Experimental studies on the behavior and capacity of concrete filled stainless steel tube short columns. Engineering Mechanics 2019;36(S1):298–305.
[44] Li D, Uy B, Aslani F, Hou C. Behaviour and design of spiral-welded stainless steel tubes subjected to axial compression. J Constr Steel Res 2019;154:67–83.
[45] Liao F-Y, Hou C, Zhang W-J, Ren J. Experimental investigation on sea sand concrete-filled stainless steel tubular stub columns. J Constr Steel Res 2019;155:46–61.
[46] Dai P, Yang L, Wang J, Gang S. Experimental study on bearing behavior of concrete-filled square stainless steel tube stub columns under axial compression. Journal of Building Structures 2019;9:1–15.
[47] Dai P, Yang Lu, Wang J, Zhou Y. Compressive strength of concrete-filled stainless steel tube stub columns. Eng Struct 2020;205:110106.
[48] He An, Su A, Liang Y, Zhao Ou. Experimental and numerical investigations of circular recycled aggregate concrete-filled stainless steel tube columns. J Constr Steel Res 2021;179:106566.
[49] Kazemzadeh Azad S, Li D, Uy B. Compact and slender box concrete-filled stainless steel tubes under compression, bending, and combined loading. J Constr Steel Res 2021;184:106813.
[50] Chen Y, Wang K, Feng R, He K, Wang L. Flexural behaviour of concrete-filled stainless steel CHS subjected to static loading. J Constr Steel Res 2017;139:30–43.
[51] Ye Y, Li W, Guo Z-X. Performance of concrete-filled stainless steel tubes subjected to tension: experimental investigation. Thin-Walled Struct 2020;148:106602.
[52] Kazemzadeh Azad S, Li D, Uy B. Axial slenderness limits for duplex and lean duplex stainless steel-concrete composite columns. J Constr Steel Res 2020;172:106175.
[53] Kazemzadeh Azad S, Li D, Uy B. Axial slenderness limits for austenitic stainless steel-concrete composite columns. J Constr Steel Res 2020;166:105856.
[54] Liu X, Wang S, Yuan B. Size effect of circular concrete-filled stainless steel tubular short columns under axial compression. Struct Design Tall Spec Build 2023;32(1):e1983.
[55] Zhong Y, Zhao Ou. Behaviour of eccentrically loaded circular recycled aggregate concrete-filled stainless steel tube stub columns. J Constr Steel Res 2022;198:107568.
[56] Han L-H, Xu C-Y, Hou C. Axial compression and bond behaviour of recycled aggregate concrete-filled stainless steel tubular stub columns. Eng Struct 2022;262:114306.
[57] Ellobody E, Young B. Design and behaviour of concrete-filled cold-formed stainless steel tube columns. Eng Struct 2006;28(5):716–28.
[58] Tao Z, Uy B, Liao FY, Han LH. Nonlinear analysis of concrete-filled square stainless steel stub columns under axial compression. J Constr Steel Res 2011;67(11):1719–32.
[59] Hassanein MF, Kharoob OF, Liang QQ. Behaviour of circular concrete-filled lean duplex stainless steel–carbon steel tubular short columns. Eng Struct 2013;56:83–94.
[60] Patel VI, Liang QQ, Hadi MNS. Nonlinear analysis of axially loaded circular concrete-filled stainless steel tubular short columns. J Constr Steel Res 2014;101:9–18.
[61] Patel VI, Liang QQ, Hadi MNS. Concrete-filled stainless steel tubular columns. Boca Raton and London: CRC Press, Taylor and Francis; 2018.
[62] Ding F-X, Yin Y-X, Mao J-F, Wang L-P, Yu Y-J, Luo L, et al. Analytical behaviors of concrete-filled circular stainless steel tubular (CFCSST) stub columns under axial loading. Structures 2019;19:277–85.
[63] He A, Zhao O. Experimental and numerical investigations of concrete-filled stainless steel tube stub columns under axial partial compression. J Constr Steel Res 2019;158:405–16.
[64] Ahmed M, Tran V-L, Ci J, Yan X-F, Wang F. Computational analysis of axially loaded thin-walled rectangular concrete-filled stainless steel tubular short columns incorporating local buckling effects. Structures 2021;34:4652–68.
[65] Yan X-F, Hassanein MF, Wang F, He M-N. Behaviour and design of high-strength concrete-filled rectangular ferritic stainless steel tubular (CFFSST) short columns subjected to axial compression. Eng Struct 2021;242:112611.
[66] Ahmed M, Gohari S, Sennah K, Chen W, Liang QQ. Computational simulation of nonlinear inelastic behavior of circular concrete-filled stainless-steel tubular short columns incorporating confinement effects. Eng Struct 2023;274:115183.
[67] Tran VL, Ahmed M, Gohari S. Prediction of the ultimate axial load of circular concrete-filled stainless steel tubular columns using machine learning approaches. Struct Concr 2023.
[68] Tran VL, Ahmed M, Gohari S. Prediction of the ultimate axial load of circular concrete-filled stainless steel tubular columns using machine learning approaches. 202200877 Struct Concr 2023.
[69] Liang QQ. Performance-based analysis of concrete-filled steel tubular beam–columns, Part I: Theory and algorithms. J Constr Steel Res 2009;65(2):363–72.
[70] Patel VI, Liang QQ, Hadi MNS. Nonlinear analysis of biaxially loaded rectangular concrete-filled stainless steel tubular slender beam-columns. Eng Struct 2017;140:120–33.
[71] Ahmed M, Liang QQ, Patel VI, Hadi MNS. Nonlinear analysis of rectangular concrete-filled double steel tubular short columns incorporating local buckling. Eng Struct 2018;175:13–26.
[72] Lin S, Zhao Y-G, Lu Z-H, Yan X-F. Unified theoretical model for axially loaded concrete-filled steel tube stub columns with different cross-sectional shapes. J Struct Eng 2021;147(10):04021159.
[73] Li Z, Lin S, Zhao Y-G. Analytical model for concrete-filled double skin tube columns with different cross-sectional shapes under axial compression. Structures 2022;43:316–37.
[74] Yu M, Hu X, Chi Y, Ye J. A unified method for calculating the fire resistance of concrete-filled steel tube with fire protection under combined loading. J Constr Steel Res 2020;168:106003.
[75] Yu M, Zha X, Ye J, Li Y. A unified formulation for circle and polygon concrete-filled steel tube columns under axial compression. Eng Struct 2013;49:1–10.
[76] Yu M, Zha X, Ye J, Wang B. A unified method for calculating fire resistance of solid and hollow concrete-filled steel tube columns based on average temperature. Eng Struct 2014;71:12–22.
[77] Lam L, Teng J. Design-oriented stress-strain model for FRP-confined concrete in rectangular columns. J Reinf Plast Compos 2003;22(13):1149–86.
[78] Légeron F, Paultre P. Uniaxial confinement model for normal-and high-strength concrete columns. J Struct Eng 2003;129(2):241–52.
[79] Attard M, Setunge S. Stress-strain relationship of confined and unconfined concrete. Mater J 1996;93(5):432–42.
[80] Quach W, Teng JG, Chung K. Three-stage full-range stress-strain model for stainless steels. J Struct Eng 2008;134(9):1518–27.
[81] Rasmussen KJ. Full-range stress–strain curves for stainless steel alloys. J Constr Steel Res 2003;59(1):47–61.
[82] Abdella K, Thannon RA, Mehri AI, Alshaikh FA. Inversion of three-stage stress–strain relation for stainless steel in tension and compression. J Constr Steel Res 2011;67(5):826–32.
[83] Lai ZC, Varma AH. Effective stress-strain relationships for analysis of noncompact and slender filled composite (CFT) members. Eng Struct 2016;124:457–72.
[84] Liang QQ, Uy B, Liew JYR. Local buckling of steel plates in concrete-filled thin-walled steel tubular beam–columns. J Constr Steel Res 2007;63(3):396–405.
[85] Ramberg W and Osgood W, "Description of stress–strain relations from offset yield strength values," NACA Technical Note no. 927, 1944.
[86] Mander JB, Priestley MJN, Park R. Theoretical stress-strain model for confined concrete. J Struct Eng 1988;114(8):1804–26.
[87] Lim JC, Ozbakkaloglu T. Stress–strain model for normal-and light-weight concretes under uniaxial and triaxial compression. Constr Build Mater 2014;71:492–509.

[88] Wang Z, Tao Z, Han LH, Uy B, Lam D, Kang WH. Strength, stiffness and ductility of concrete-filled steel columns under axial compression. Eng Struct 2017;135:209–21.
[89] Oehlers DJ, Bradford MA. Elementary behaviour of composite steel and concrete structural members. Oxford U.K.: Butterworth-Heinemann; 1999.
[90] AS/NZS 4673-2001. Cold-formed Stainless Steel Structures. Australian/New Zealand Standard, Sydney, NSW, Australia. 2001.
[91] Li L. Structural performance of concrete-flled cold-formed stainless steel members. China, Hong Kong: The University of Hong Kong; 2017.
[92] Ding F, Fu L, Yu Z, Li G. Mechanical performances of concrete-filled steel tubular stub columns with round ends under axial loading. Thin-Walled Struct 2015;97:22–34.
[93] Piquer A, Ibañez C, Hernández-Figueirido D. Structural response of concrete-filled round-ended stub columns subjected to eccentric loads. Eng Struct 2019;184:318–28.
[94] Tao Z, Wang Z-B, Yu Q. Finite element modelling of concrete-filled steel stub columns under axial compression. J Constr Steel Res 2013;89:121–31.
[95] Katwal U, Tao Z, Hassan MK, Wang WD. Simplified numerical modeling of axially loaded circular concrete-filled steel stub columns. J Struct Eng 2017;143(12):04017169.